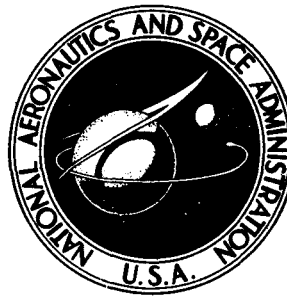


**NASA CONTRACTOR
REPORT**



NASA CR-2894

NASA CR-2894

**AAFE LARGE DEPLOYABLE
ANTENNA DEVELOPMENT PROGRAM**

Executive Summary

Prepared by

HARRIS CORPORATION

Melbourne, Fla. 32901

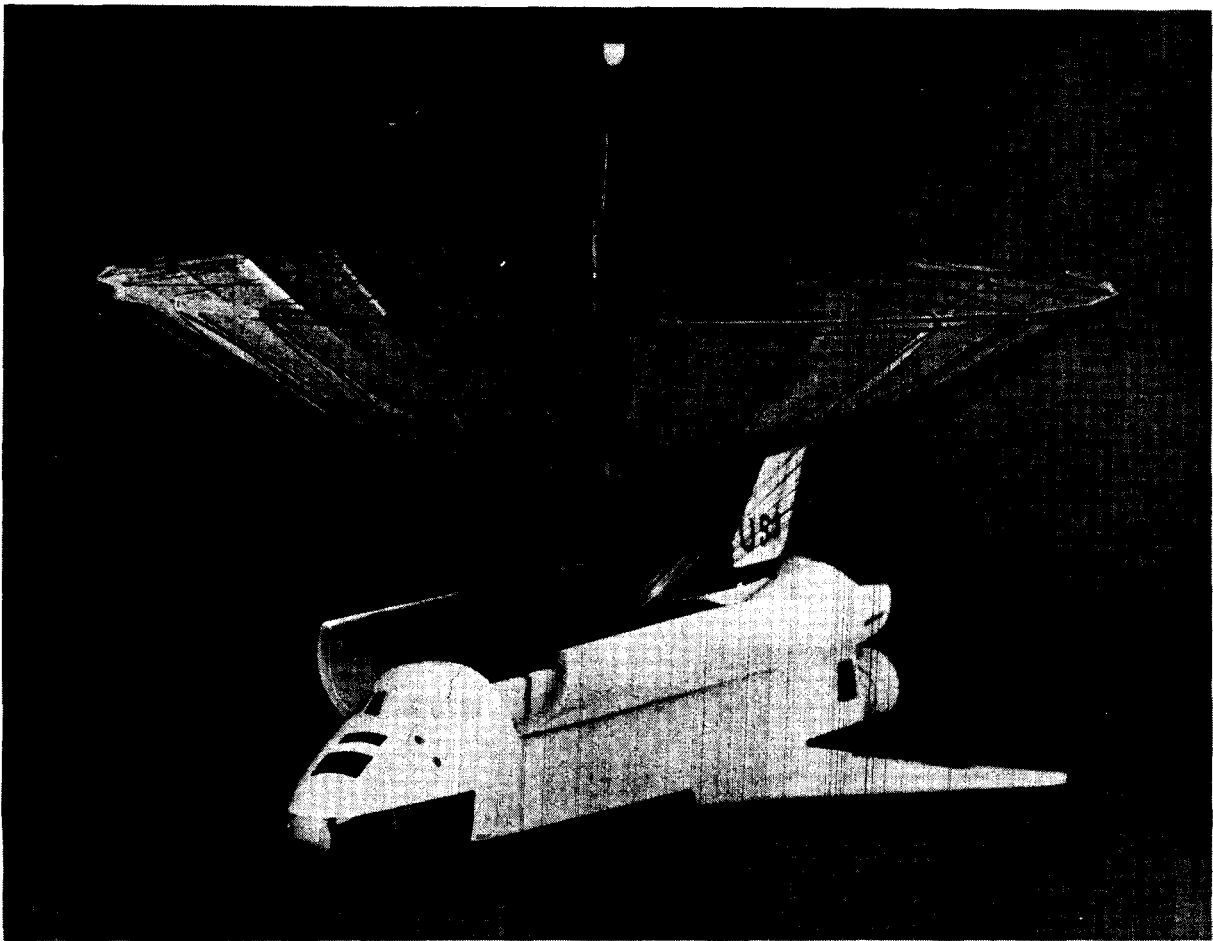
for Langley Research Center

NATIONAL AERONAUTICS AND SPACE ADMINISTRATION • WASHINGTON, D. C. • OCTOBER 1977

FOREWORD

This report summarizes the work done and results obtained under NASA Contract NAS1-13943 "Design Development of Large, Extremely Lightweight, Erectable Space Antennas." This AAFE

program was monitored through the NASA Langley Research Center, Hampton, Va., by Mr. Thomas G. Campbell Contract Technical Representative. Any inquiries relating to this program should be directed to Mr. Campbell.



Photograph of 30-Meter Diameter Reflector Antenna Deployed from Shuttle

INTRODUCTION

This program was initiated as a result of NASA foreseeing future requirements for large diameter deployable space antennas. Identification of potential users in fields of communications, earth observation, RFI detection, radio astronomy, deep space probes, and microwave energy transmission, have substantiated the need for these antennas. The requirements of the users and of specific missions (e.g., the Large Deployable Antenna Shuttle Experiment (LDASE)) have been used as the guidelines for the program.

The objective of this program was to develop a design concept of a large diameter (10 to 100 m) deployable, parabolic antenna for space applications, and to establish the feasibility of this concept. This was to be accomplished through detailed mechanical design, analytical performance predictions and the demonstration of a working engineering model.

Design performance objectives generated from the identified user requirements are shown in Figure 1. These objectives represent typical performance goals used to both guide and constrain the design.

- **DESIGN APPLICABLE TO A WIDE RANGE OF APERTURE DIAMETERS (10 TO 100 m)**
- **STOWED PACKAGE SIZE CONSISTENT WITH SHUTTLE PAYLOAD VOLUME**
- **HIGH SURFACE ACCURACY (12.7 mm RMS FOR 30 m)**
- **CAPABLE OF BEING RESTOWED AFTER DEPLOYMENT**
- **LIGHTWEIGHT DESIGN**

Figure 1. Design Performance Objectives

This report summarizes the methods used in meeting the objectives, the results and accomplishments of the program, and detailed descriptions of the concept and its method of operation.

Program Summary

During the first stage of the program, the preliminary design phase, many candidate design concepts were generated and considered. Once defined, these concepts underwent design changes directed at optimizing them prior to the selection of a single baseline concept. Of the many concepts studied, four were chosen to be examined in detail. Further design work continued on these four concepts until an evaluation of the concepts relative to each other could be made. Trade-off studies were performed and a single concept was selected as the baseline. (See Appendix A for details.)

A 1.82 m diameter engineering model of this concept was built to verify feasibility and aid in uncovering design problems. After completing concept verification demonstrations of the model, the second stage of the program, or detailed design phase, was initiated.

This phase entailed a concentrated design effort on the selected concept. Loads were generated, materials were selected, members were sized and weight budgets were calculated. Structural, dynamic, and thermoelastic analyses were performed. The calculated distortions resulting from these analyses plus the estimated manufacturing tolerances and other error sources formed the basis for predicting surface accuracy and RF performance. Detailed design drawings were made of the baseline concept for three aperture diameters in the range of interest (15, 30, and 100 m).

Results

The Hoop/Column concept shown in Figure 2 was selected as the baseline concept. This design concept met all of the established program objectives, and offered many advantageous features not specifically defined. For example, the stowed dimensions of the antenna can be varied to obtain the desired form factor by changing the number of segments in the hoop. Also, a highly efficient structural design resulted through the use of structural members being loaded in tension or compression only. A major breakthrough in "Maypole" type antennas was achieved by the use of a rigid rather than a flexible hoop where stability is no longer a problem.

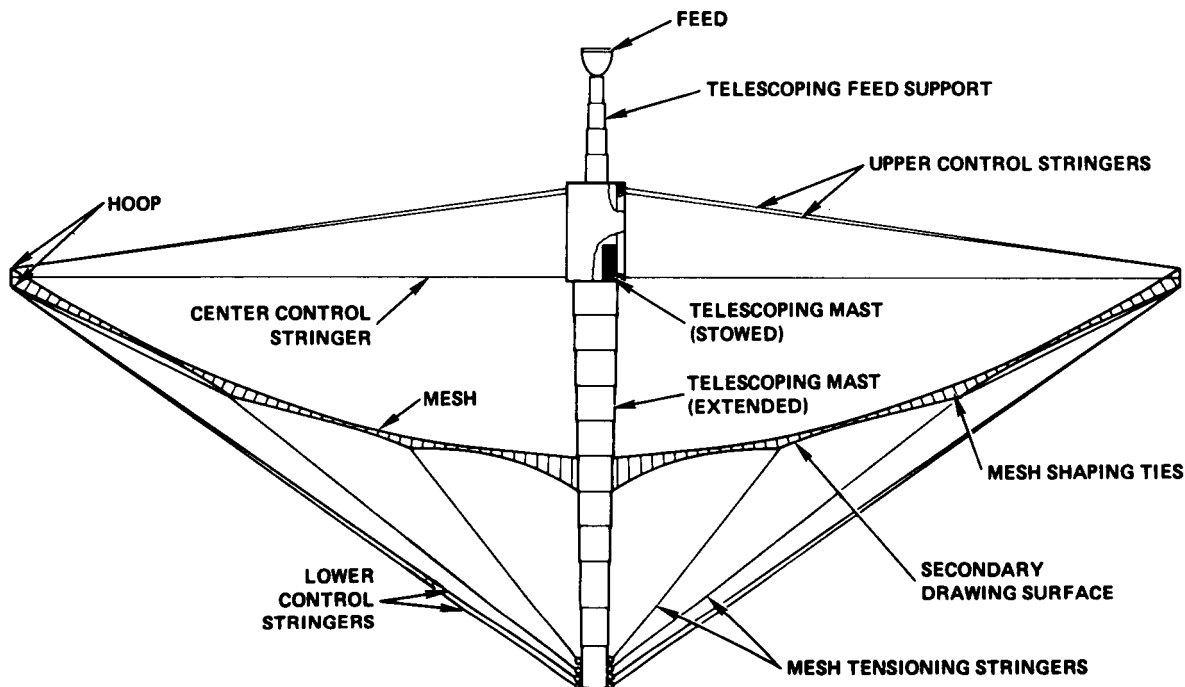


Figure 2. Hoop/Column Concept

In addition, evaluations of the demonstration model (Figure 3) and of the detail layouts for the three aperture diameters (15 m, 30 m, and 100 m) have shown no inherent size limitation other than the available volume for the stowed aperture. Since the stowed packaging geometry is very favorable from a stowed package volume-to-aperture diameter standpoint, the available volume for the stowed package is not a significant constraint, especially for shuttle launches.

The basic mechanical design also has potential applications for space structures other than parabolic antennas. Examples include spherical reflectors, phased arrays, lenses, solar arrays and structural platforms.

Concept feasibility was established through hoop deployment demonstrations using a 1.82 m diameter engineering model (Figure 3). This model also provided insight into the concept's mesh handling characteristics and potential design problems.

Performance predictions based on the results of analysis present a good assessment of the antenna's

overall capabilities. A brief summary of these predictions is shown in Table 1.

Table 1. Summary of Performance

DIAMETER PARAMETER	15 m	30 m	100 m
WEIGHT	172 kg (378 LBS)	341 kg (753 LBS)	1530 kg (3374 LBS)
SURFACE ERROR mm RMS (MANUFACTURED)	7.62	14.99	50.04
PROJECTED GAIN, dB 4 GHz	54.3	59.8	64.9
LOSS, dB	1.60	2.02	7.49

The end result of this program is a low cost, lightweight, deployable antenna design, the Hoop/Column concept, which has high packaging efficiency and high surface accuracies throughout the range of aperture diameters.

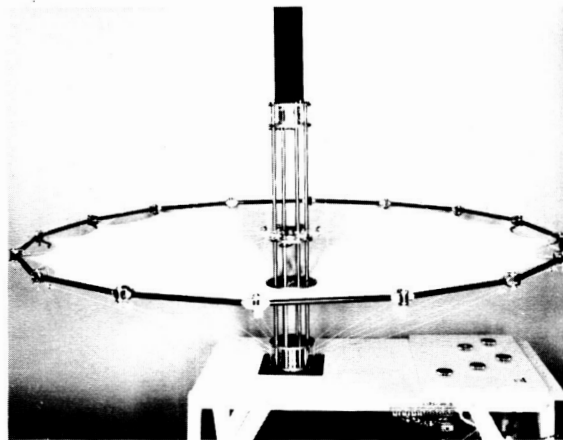
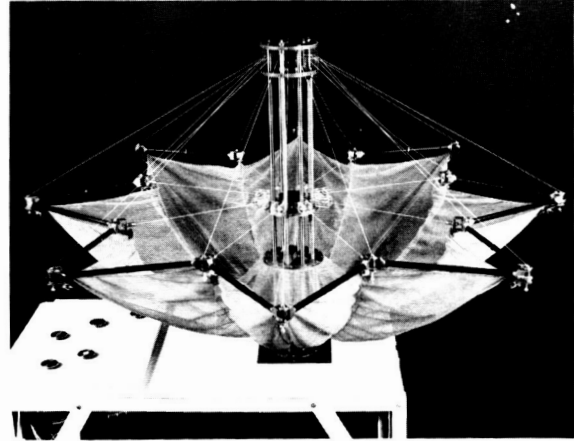
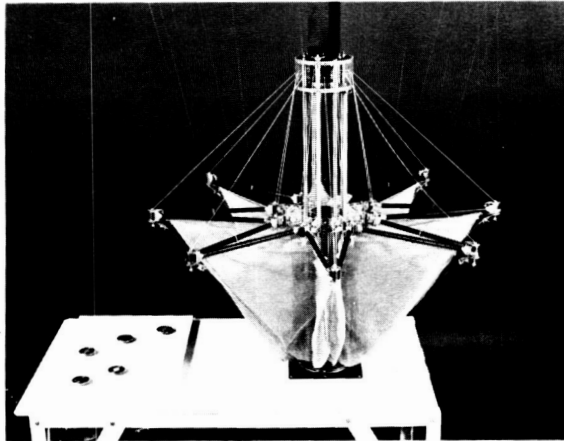
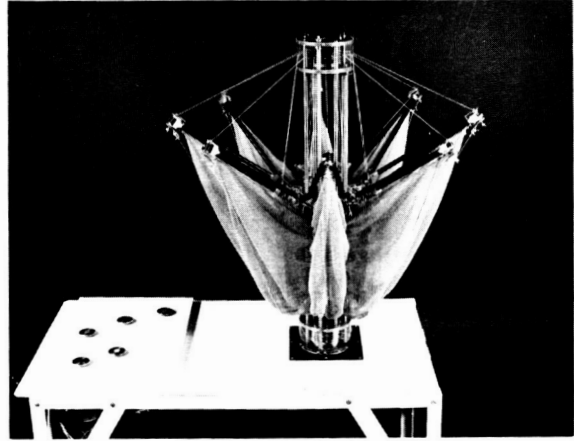
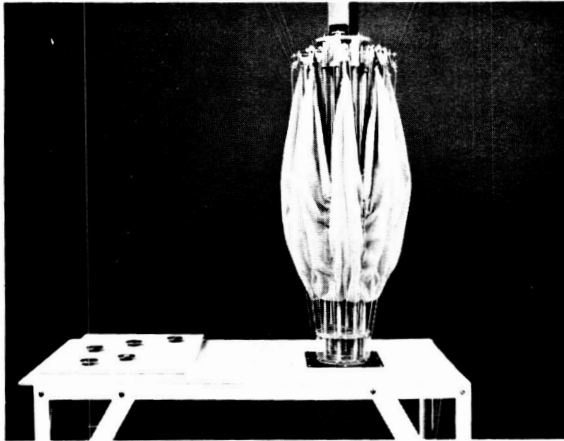


Figure 3 Hoop/Column Reflector Demonstration Model

DESIGN DESCRIPTION

The description given below and throughout the remainder of this report is for a 30 meter diameter antenna unless specified otherwise. The number of hoop segments (40) is based on an iterative process which is described below. The 15 m and 100 m diameter antenna designs, for which performance estimates are made, use the same number of hoop segments for consistency and comparability only. The actual number of joints for these antennas in practice is a function of the packaging volume available and form factor requirements of the launch vehicle.

Major Elements

The major elements of the Hoop/Column concept are shown in Figure 2. A brief description of these elements and their functions follows:

Hoop — The hoop's function is to provide a rigid, accurately located, structure to which the reflective surface attaches. It is comprised of 40 rigid sections which articulate at hinges joining each adjacent segment. These segments consist of two tubular graphite fiber reinforced plastic (GFRP)

members parallel to each other and attached to a long hinge member at each end. The long hinges allow the separation between the tubular members required by the geometry of the mesh-secondary drawing surface combination which is described later. Torsion springs are located in every hinge and supply the total energy required to deploy the hoop.

On this program, the initial stowed configuration design goal was generated from the requirements of the Large Diameter Antenna Shuttle Experiment (LDASE). This requirement stated that a 30 m antenna must fit vertically on a single spacelab pallet, as shown in Figure 14. This allowed a stowed height of approximately 3.35 m. The process used to select the number of hoop segments which permits the most efficient use of the available packaging space is described below.

The fewest number of hoop segments possible which allow compatibility with the packaging volume available, is the optimum number from a control and complexity standpoint. The dimensions needed to determine acceptability of a given configuration are shown in Figure 4.

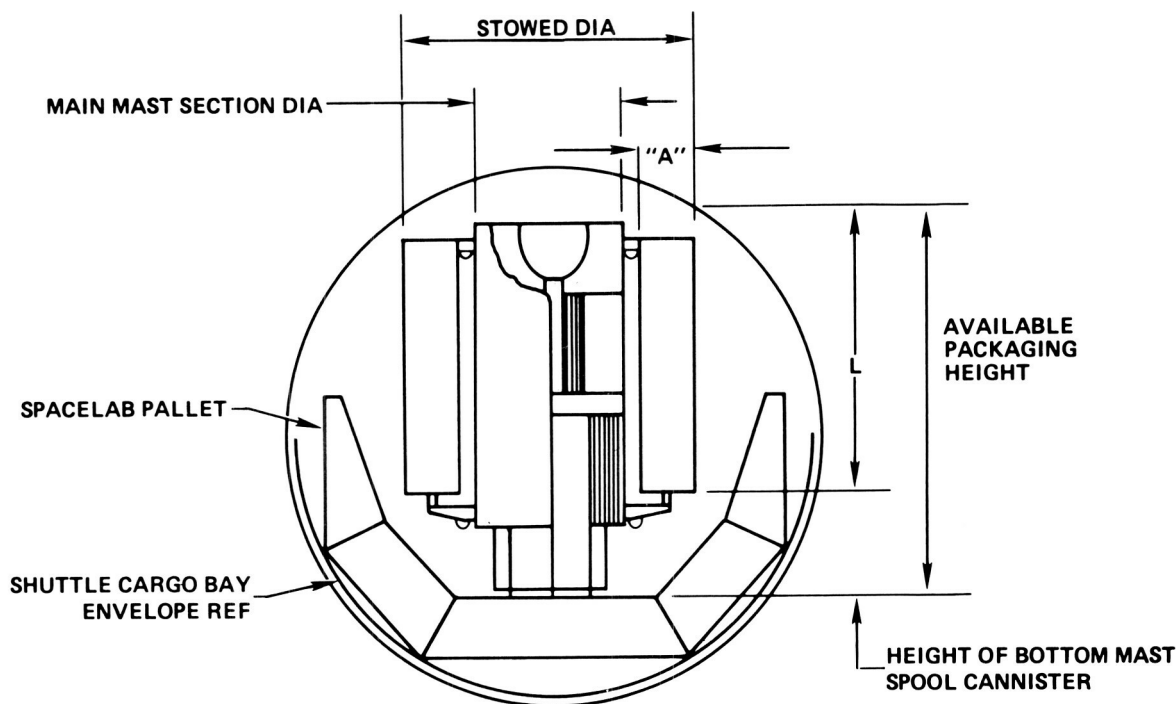


Figure 4. Form Factor Determination

The number of hoop segments must be determined first. A close approximation of this number can be made by using the available packaging height minus the height of the bottom mast spool cannister as the length of the hoop segment. The number of segments can then be found from

$$L = 2 (\text{Antenna Radius}) \sin \frac{360}{2N}$$

or

$$N = \frac{360}{2 \arcsin \frac{L}{2(R)}}$$

The stowed diameter is then found by multiplying 1/2 the number of segments times a nominal spacing which allows for clearance between adjacent hoop sections. This results in the circumference of the main mast section. The diameter of this section can then be found.

The "A" dimension or the length of the hinge member is determined next. This dimension is a function of the geometry of the antenna and results from the clearance requirements of the mesh-secondary drawing surface combination. Once it is determined, it is doubled and added to the diameter of the main mast section. The result is the stowed diameter of the antenna.

These dimensions are rechecked against the available packaging space. If the dimensions are not satisfactory, the process is repeated using a different number of hoop segments.

Mast — The central column or mast is extendable and contains the microwave components and control mechanisms. It consists of tubular GFRP shell members which nest inside each other when in the stowed position. Structural rings are attached to each end of the sections and provide attachment points for the mechanism required to extend the mast. This operation is described later.

Aside from housing various components, the mast provides attachment locations for the reflective surface and the stringers.

Stringers — There are five sets of stringers used on the Hoop/Column concept. Three of these sets

are used for hoop deployment control and the other two sets are used for mesh shaping.

The hoop control stringers are located at the upper end of the main mast section, the lower portion of the main mast section and the lower end of the extendable mast section. These stringers are located around the mast at the positions described and extend radially outward to their attachment positions at the hinges of the hoop. The upper and lower control stringers function in an analogous manner to the spokes of a wheel. They accurately and rigidly position the hoop throughout its deployment. The center control stringers are used in deployment rate control and in pulling the hoop joints toward the center mast during the stowing sequence.

The remaining two sets of stringers (mesh tensioning stringers) are located just above the lower control stringers and are used in shaping the reflective surface into the proper contour.

All of these stringers are made of stranded quartz cords. This material has high stiffness along with exceptional thermal stability.

Reflective Surface — The reflective surface is produced by properly shaping a knitted mesh fabric. The mesh is made of 1.2 mils diameter molybdenum wire which is gold plated prior to being knitted. This ensures plating uniformity which is necessary for obtaining uniform mechanical properties. It also yields low contact resistance and high conductivity which are both necessary for good RF reflectivity.

The structure which permits proper shaping of the mesh consists of numerous radial quartz stringers (Figure 5) to which the mesh is attached (mesh surface stringers) along with a similar set of stringers (secondary drawing surface stringers) positioned beneath them. Short ties (mesh shaping ties) made of fine Invar wire connect the mesh surface stringers to the secondary drawing surface stringers as shown in Figure 6. When the mesh tensioning stringers are tensioned, they in turn tension both the secondary drawing surface stringers and the mesh shaping ties to produce an essentially uniform pressure distribution on the mesh. This pressure allows uniform shaping of the mesh to a parabolic curvature. This configuration is shown for a single gore element in Figure 7.

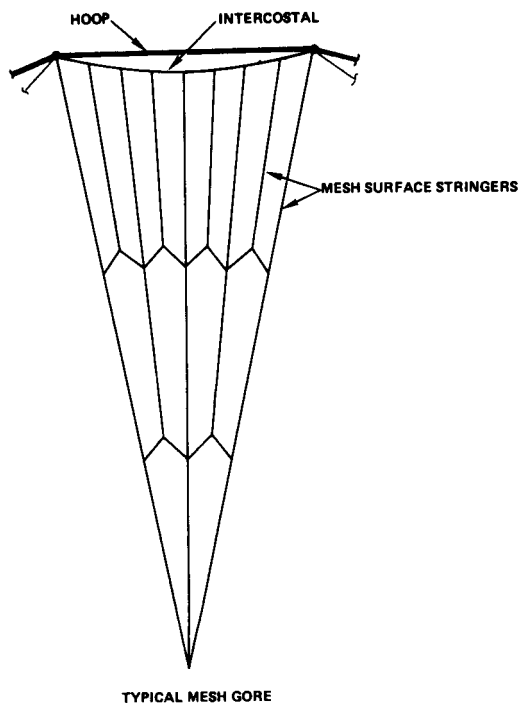


Figure 5. Mesh Surface Stringer Configuration

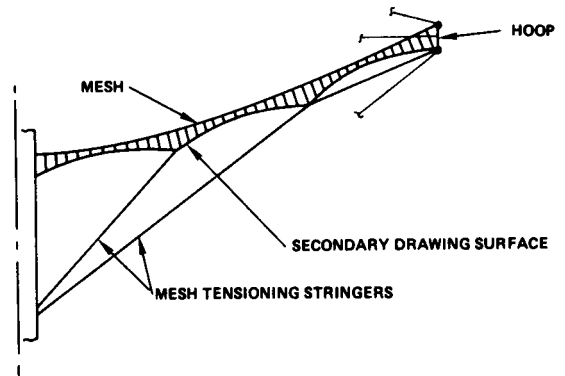


Figure 6. Mesh Shaping Technique

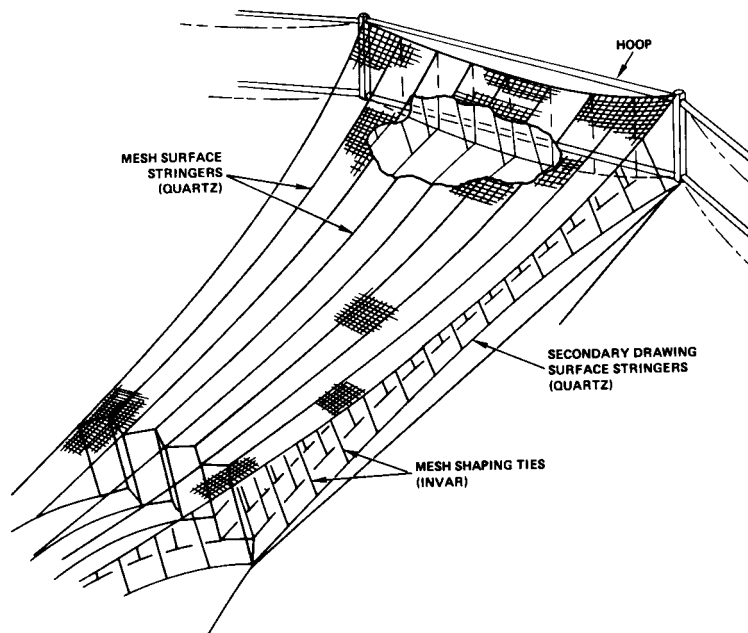


Figure 7. Mesh Shaping Configuration

The surface accuracy is affected by the number and spacing of the mesh shaping ties. The greater the number of ties, the greater surface accuracy.

Drive Mechanisms – There are two groups of drive mechanisms used in the Hoop/Column concept. One group is used to extend the mast and the other group is used to adjust the control stringers.

The drive mechanisms used for extending the mast consist of one basic set of mechanisms for each section of the telescoping mast. Each set contains three Acme threaded rods, a chain, three sprockets, a torque motor and clutch. The Acme threaded rods are attached to the flanges of the structural rings of each section and are aligned parallel to the axis of the mast. They are equally spaced around the mast and joined together by means of the chain and sprockets. The motor drives a single rod which in turn drives the remaining two. The method of operation is fully discussed later in the report.

The second group of drive mechanisms contains spools to which the stringers attach and torque motors which drive the spools. There are five sets of spools, one for each group of stringers. The spools are used to wind up and pay out the stringers during the deployment and stowing

sequence. They are positioned around the mast in the locations described for the stringer attachments. A torque motor drives each set of spools independently as required by the particular position and velocity of the hoop joint being controlled. The spools of each set are connected in series by sliding universal joints. A worm and wheel gearbox with a 250:1 gear reduction is attached to the spools and is driven by the torque motor. This high gear reduction in a worm and wheel gearbox does not allow the system to be back-driven and eliminates the need for a brake.

Control System – The control system logic is depicted by the block diagram shown in Figure 8. The heart of the system is the controller, which consists of either a microprocessor or discrete logic circuitry. It both controls and configures the individual servos as well as outputting status data. Typical control outputs would be position commands, rate commands, and tension commands. Configuration outputs would be to set the servos to position, rate, or tension control modes. The controller has the additional capability of adaptively adjusting loop compensation as a function of deployment stage to optimize performance. Its final function would be to check for system failures and switch to redundant equipment if necessary.

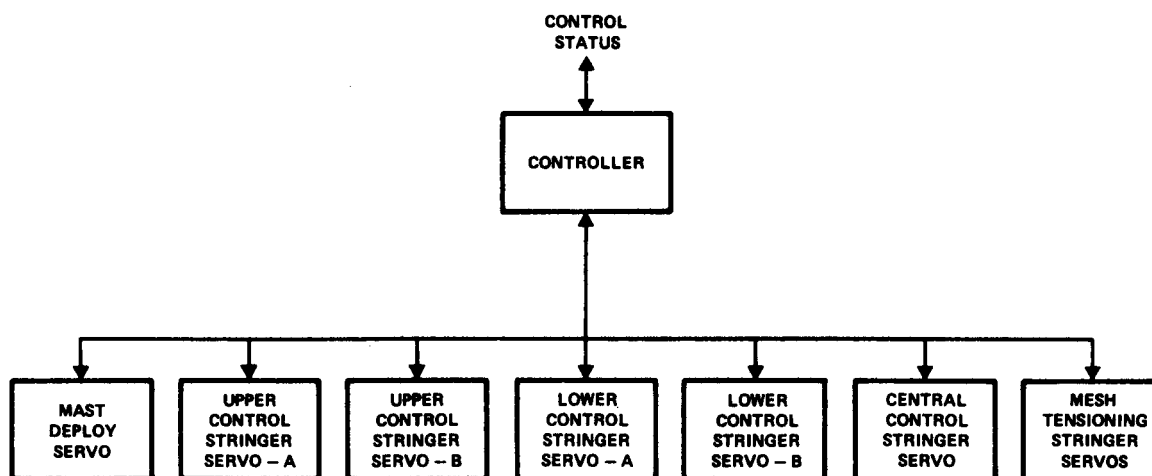


Figure 8. Deployment Control System

A typical stringer control servo logic diagram is shown in Figure 9. The servo is capable of adaptive configuration and loop adjustment. It utilizes dc

and lower flanges of the adjacent section. Figure 12 shows this arrangement and the mast extension process schematically. The rods are allowed to

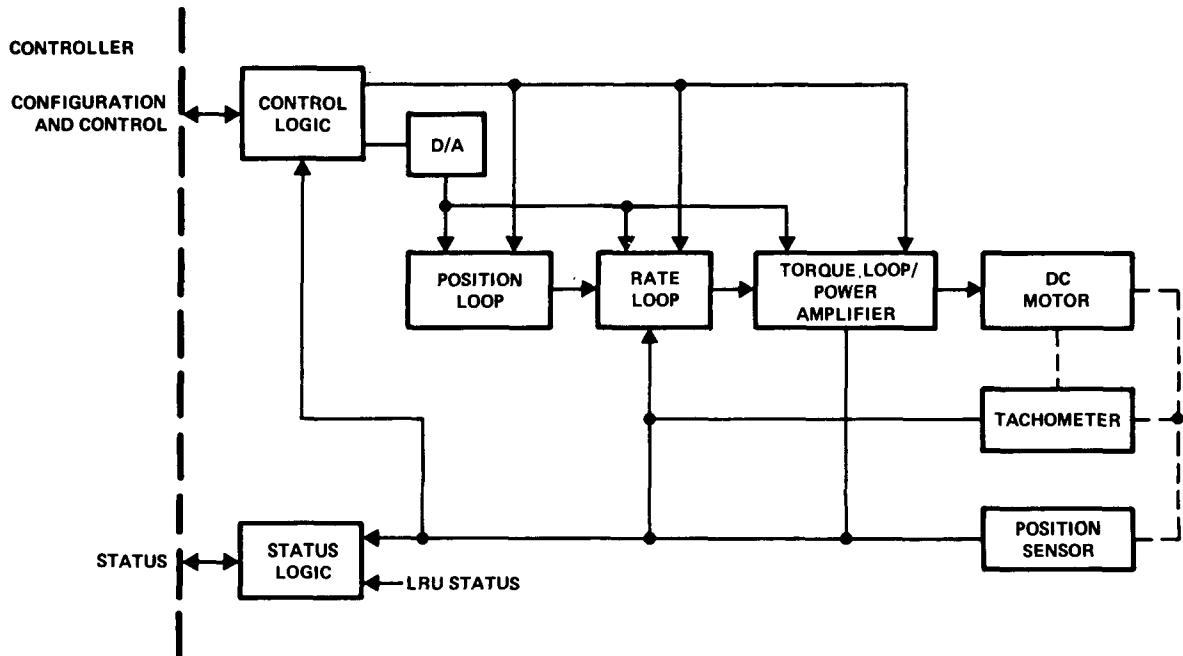


Figure 9. Typical Stringer Control Servo

motors which can be either speed, torque, or position controlled. It is also able to encode the stringer spools to both monitor and control position.

Deployment Sequence

In the launch configuration, the antenna is packaged in its stowed position. The hoop is folded around the main mast section as shown in Figure 10. The feed mast and the lower mast sections are retracted inside this main section. The area beneath the hoop and around the lower mast section houses the mesh. The mesh is loosely packaged in this area, and confined by the lower control stringers. The volume available for the mesh relative to the volume required to stow it without causing any permanent set is approximately 10:1.

The deployment sequence begins with the extension of the telescoping masts, as illustrated in Figures 11a and 11b. The inner mast section is driven away first. Acme threaded rods are attached to the lower flange of the inner section and to the upper

rotate on the flanges of the adjacent sections, but are restrained from axial motion. The lower flange of the inner section is threaded to mate with the Acme threaded rod. As the rod turns, the inner section is driven out until its flange bottoms out against the flange of the adjacent section. The sequence is then repeated until all sections are deployed.

As the mast is extending, the lower stringers are payed out from their respective spools to compensate for the increased length. Once the mast is fully extended, the hoop deployment sequence begins.

This sequence begins by the upper control stringers which are attached to hoop joints in the uppermost position (joints A) being payed out of their respective spools. This allows these joints to move away from the mast as shown in Figure 11c. They translate outward and down as they rotate about the fixed position of the lower joints (joints B) until all of the hoop members lie in one plane perpendicular to the mast. This motion is caused by torsional strain energy forcing the members to

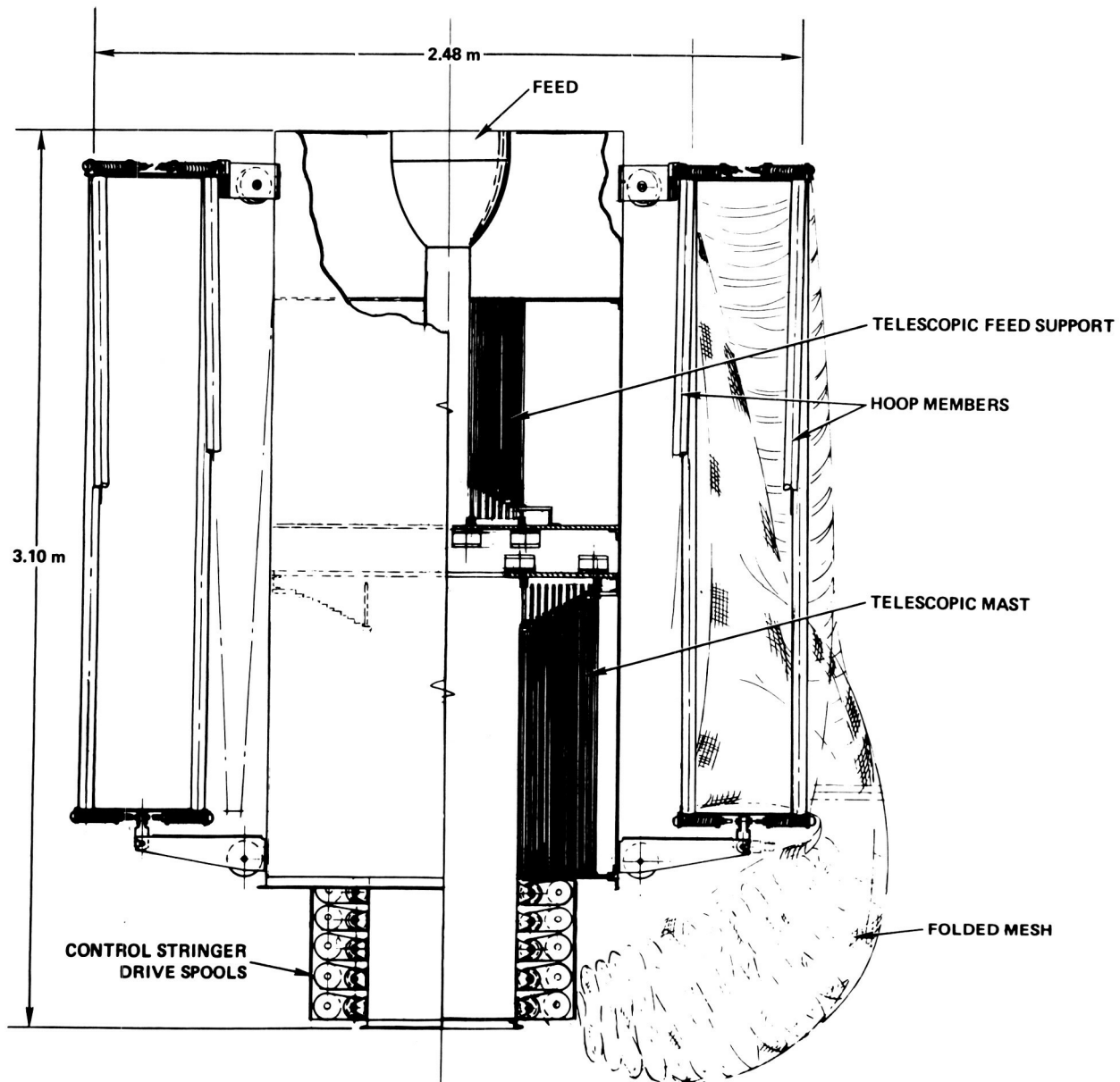


Figure 10. 30-Meter Antenna Stowed Configuration

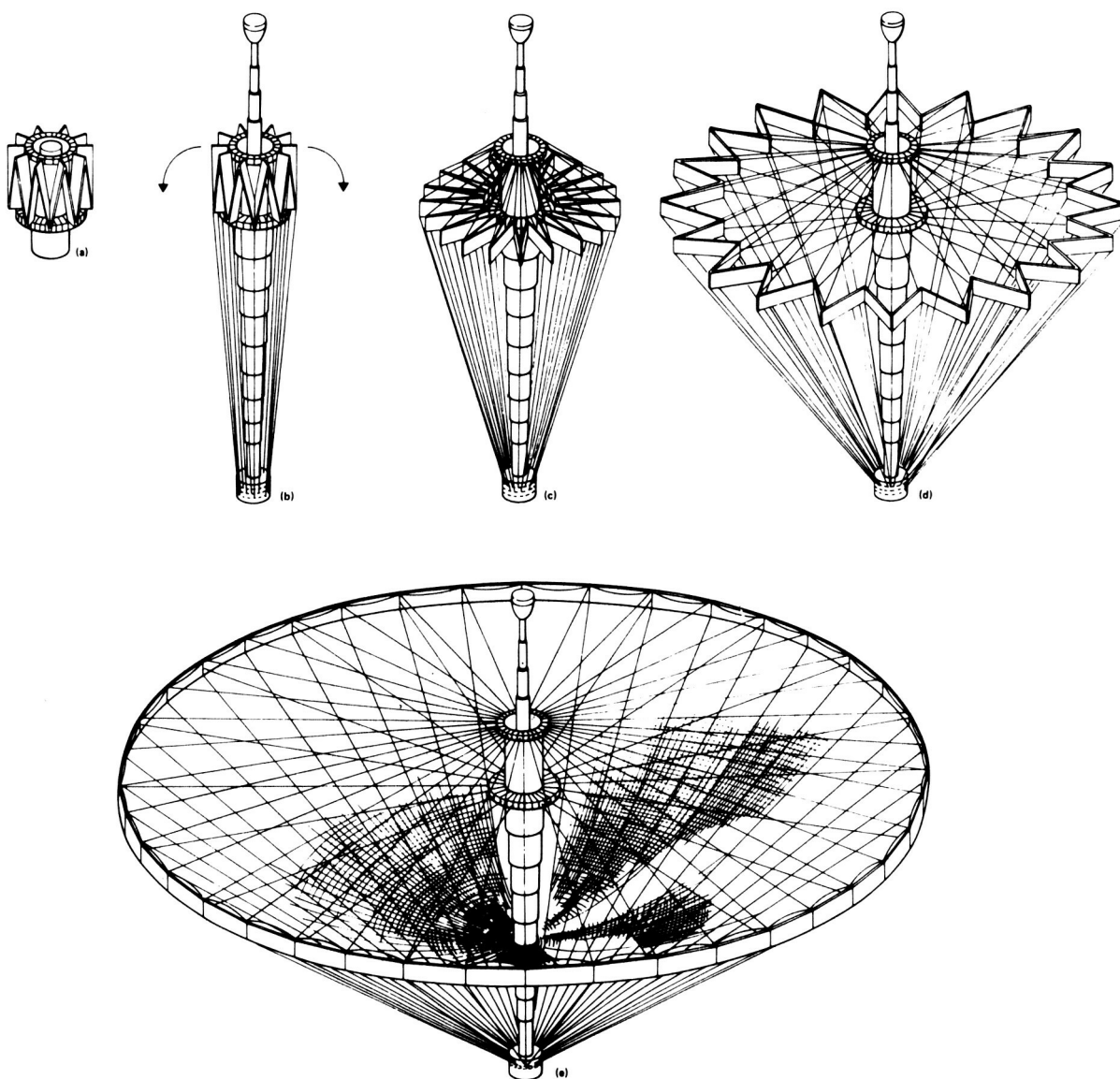


Figure 11. Deployment Sequence

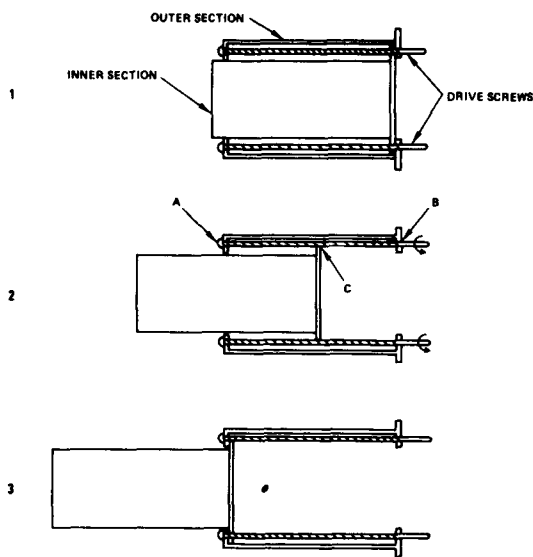


Figure 12. Telescopic Mast Operation

untwist and seek an equilibrium position. This can be understood by observing that when the hoop is in the planar position, all of the axes of the hinges are parallel. In the fully stowed position, however, these same hinge axes all point radially inward. This motion causes torsional strain energy to be

stored in the hoop members as they twist through approximately 90° .

The next stage of hoop deployment takes place by paying out all of the control stringers, each set at its own rate. The torsion springs in each hinge joint act on those hoop members adjacent to each joint in such a manner that the angle formed between these hoop members tends to increase. This can be seen in Figure 13. The springs in joints A tend to make the angles α increase and likewise, the springs in joints B tend to make the angles β increase. Due to the regular geometry of the hoop, the resultant hoop forces are radially outward applied at the joints. Equilibrium is maintained by reacting these forces with the control stringers.

As the control stringers are payed out, the hoop forms an increasingly wider star pattern until just prior to full deployment. See Figure 11d. As the hoop nears its final position, the inner joints, joints B, pass through the center of action of the adjacent joints (angle β becomes greater than 180°) until they reach their maximum position. At this position the hoop forms a regular 40-sided polygon approximating a circle as shown in Figure 11e. All of the hoop joints have mechanical stops which prevent further motion of the hoop.

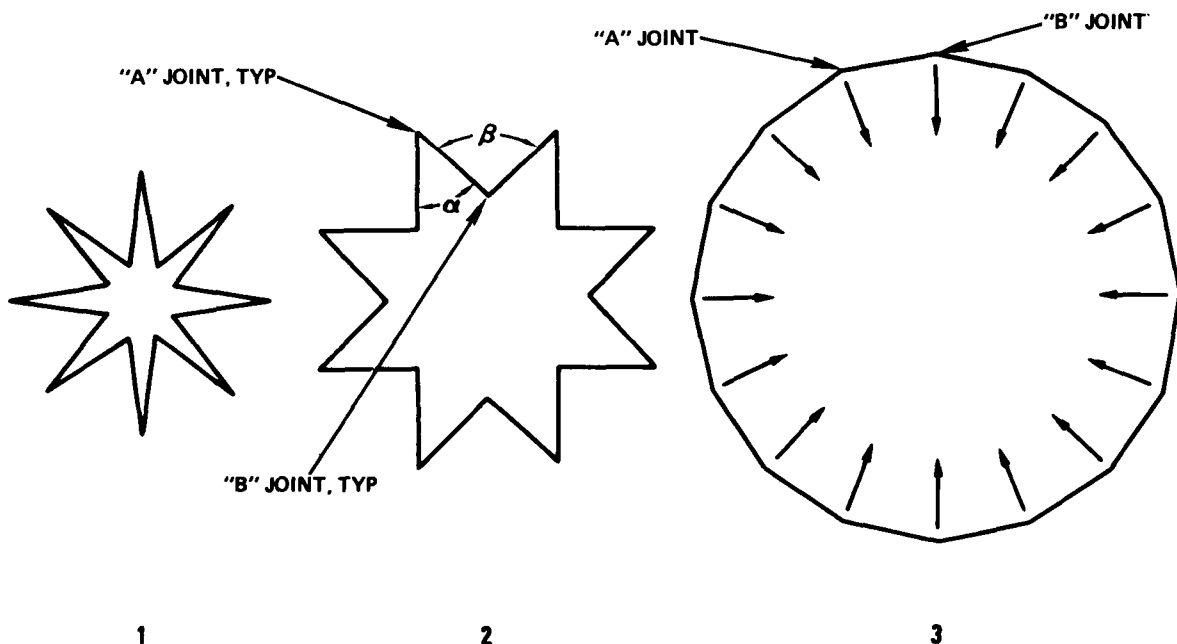


Figure 13. Hoop Deployment Sequence

When the hoop is in this fully deployed position, the upper stringers have been completely payed out of their spools. At this point, the lower control stringers are tensioned causing an axial compression load in all the hoop members. The vertical component of the tensile load in the lower stringers is reacted by the upper stringers, which results in their being loaded in tension. The net effect is an extremely rigid overall structure.

The final stage in the deployment sequence is the shaping of the reflector surface. This is accomplished by tensioning the mesh tensioning stringers by reversing the lower spools to which they are attached. This process tensions the secondary drawing surface stringers and the mesh shaping ties effecting a uniform pressure distribution over the mesh. This pressure allows for the uniform shaping of the mesh to the desired parabolic contour.

The stowing sequence is the exact reverse of the process just described.

Significant Features

There are many significant features of the Hoop/Column concept which aided in it being selected as the baseline approach.

The design is extremely lightweight and packages into a compact stowed size. This stowed volume is dependent upon the number, and hence, the length of the individual hoop segments. For a given aperture diameter, the fewer the number of segments there are, the larger the stowed length and smaller the stowed diameter will be and vice versa. On this program, the hoop was designed with 40 segments to allow a 30 m antenna to fit on a single spacelab pallet within the space shuttle as shown in Figure 14. Other launch vehicles might require the same

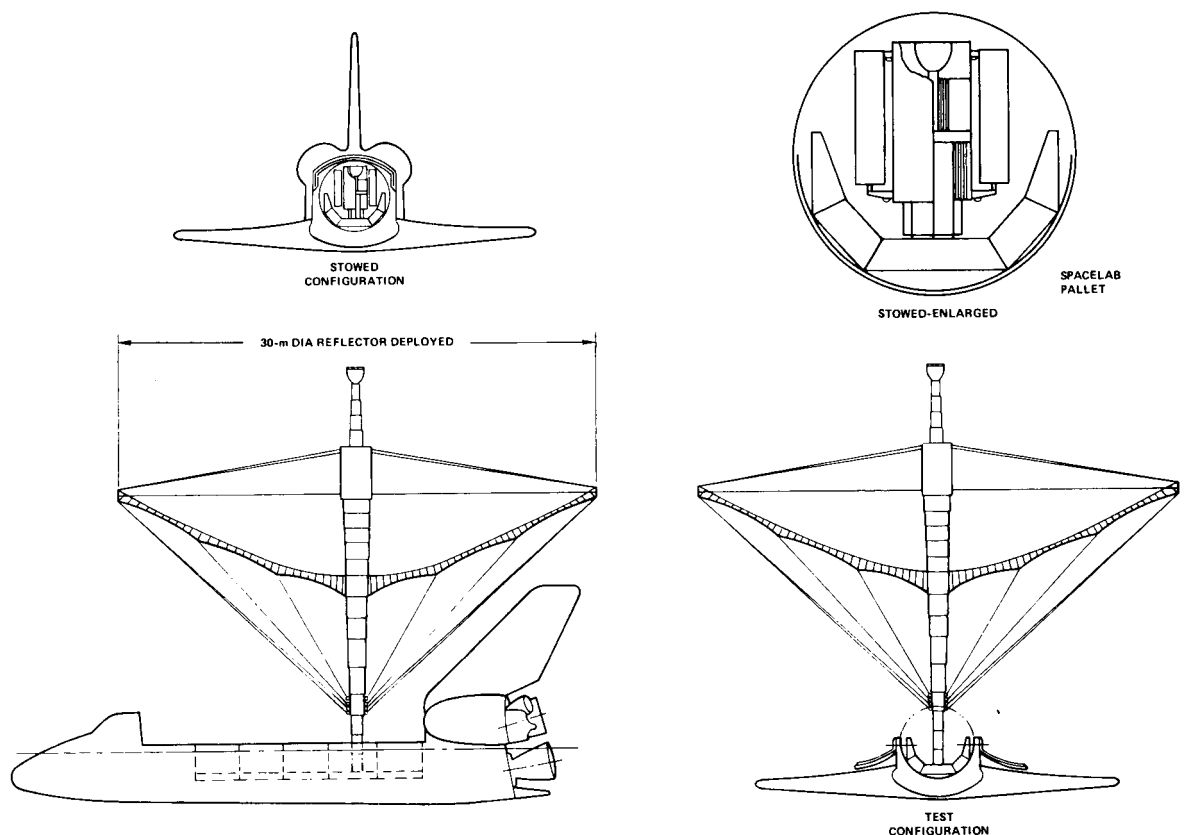


Figure 14. LDASE Configuration

diameter antenna to have more or fewer segments in the hoop depending on their particular payload volume requirements.

The design is highly efficient structurally. All structural members are loaded in either tension or compression as opposed to bending. This is significant in that deflections are smaller, more repeatable, and more accurately predictable than deflections under bending loads. Tension members have the additional advantage of being nonstability critical, and, therefore, generally smaller in size and lighter in weight.

Also, because the individual hoop segments are rigid, there is no requirement to stabilize any points of the hoop other than the articulating hinge joints. This is a significant advantage over flexible hoop concepts because those points on a flexible hoop which are stabilized by stringers, are no different structurally than any other point on the hoop. Hence, they are inherently unstable under a compressive load between the stabilized points.

The mesh shaping structure is made of lightweight high modulus, thermally stable materials. This structure permits the accurate shaping of the mesh, and hence, high surface accuracy, while eliminating the influence of varying tension fields in the mesh.

The energy for hoop deployment is supplied by torsion springs located in each hinge joint of the hoop. This is a highly redundant system which greatly increases the reliability of the deployment process. It is redundant in that if all of the springs in either the inner or outer joints were removed, the hoop would still deploy due to the remaining springs and the symmetrical geometry of the deployment pattern.

The energy requirements and hence the sizes of these springs are minimized by the fact that the hoop does not have to stretch the mesh. This operation is done only after full hoop deployment and preload.

The concept exhibits completely controlled deployment throughout that sequence. The motion is relatively slow with no rapid or violent actions. The reliability and repeatability of the concept is thereby greatly enhanced.

Materials selected for the various components of the Hoop/Column concept were carefully considered for their mechanical and thermal properties and the specific applications for which they would be used. Quartz was chosen for the stringers due to its high modulus of elasticity and its extremely low coefficient of thermal expansion. Because of these properties and the relatively low stress levels to which the stringers are loaded, the thermal and structural deflections are very low, ensuring high positional accuracy. GFRP was selected for similar reasons for applications in the hoop members and mast sections.

A final and very significant feature of the concept is that the basic design has no inherent size limitations. The only constraint is the volume available in the launch vehicle. Since the design has a very favorable stowed package volume-to-aperture diameter, the constraint of available volume is not a significant constraint, especially for shuttle launches.

FABRICATION AND ASSEMBLY

When a deployable antenna of moderate size (up to 20 m diameter) is fabricated, the reflector is fully assembled and then adjusted and evaluated. The measurements and tests performed on the full reflector provide a realistic baseline from which to predict on-orbit performance. This will not be feasible with very large diameters (30 m and greater) since:

- A facility large enough to accommodate a full reflector of this size will not likely be available.
- Large lightweight reflectors designed for zero-g operation generally do not have sufficient strength and stiffness to permit a meaningful evaluation on the ground.

Because of these reasons, the proposed fabrication and assembly method is a "build-to-dimension" technique which involves multiple subassemblies of reasonable size that can be adjusted individually prior to final assembly. The size of the subassembly is determined by choosing a representative element that occurs at a natural division of the antenna. For example, a complete gore will be assembled at one time for a 30-meter diameter antenna and a

half gore will be the elemental size for a 100-meter antenna.

The following fabrication and assembly sequence description is based on a 30-meter diameter antenna. The process is also applicable to both larger and smaller diameters, and is depicted by the flow chart shown in Figure 15.

The mesh fabrication sequence is shown in Figure 16. A flat pattern template of the individual gore element of the parabolic reflective surface is positioned on a large flat table (mesh tensioning table). The locations of all the mesh ties are marked on this template. A rectangular piece of mesh is then positioned on the table, covering the template. Weights attached to the mesh along each edge are used to stretch the mesh to its proper tension levels of $1.77 (10^{-5})$ kg/mm radial tension by 3.54×10^{-5} kg/mm circumferential tension. The table is then vibrated to relieve any frictional resistance between the mesh and the table. The gore edges

and tie locations are marked on the mesh using the template and the pattern is cut out. The process is then repeated for all the gores required. Later, when the gores are attached to each other and deployed to the proper shape on the antenna, the tension field in the mesh is the same as when fabricated on the mesh tensioning table.

The intercostals, ties, and all stringers are fabricated by cutting them to their proper lengths which are predetermined precisely from the geometry of the antenna. Connector terminations are attached to these cords on tooling designed to maintain their proper length.

Upon completion of piece part fabrication, assembly of each individual unit begins. A fixture such as the one shown in Figure 17 is used to assemble a single gore secondary drawing surface combination. Accurately located standoffs on the fixture simulate the hoop hinge locations.

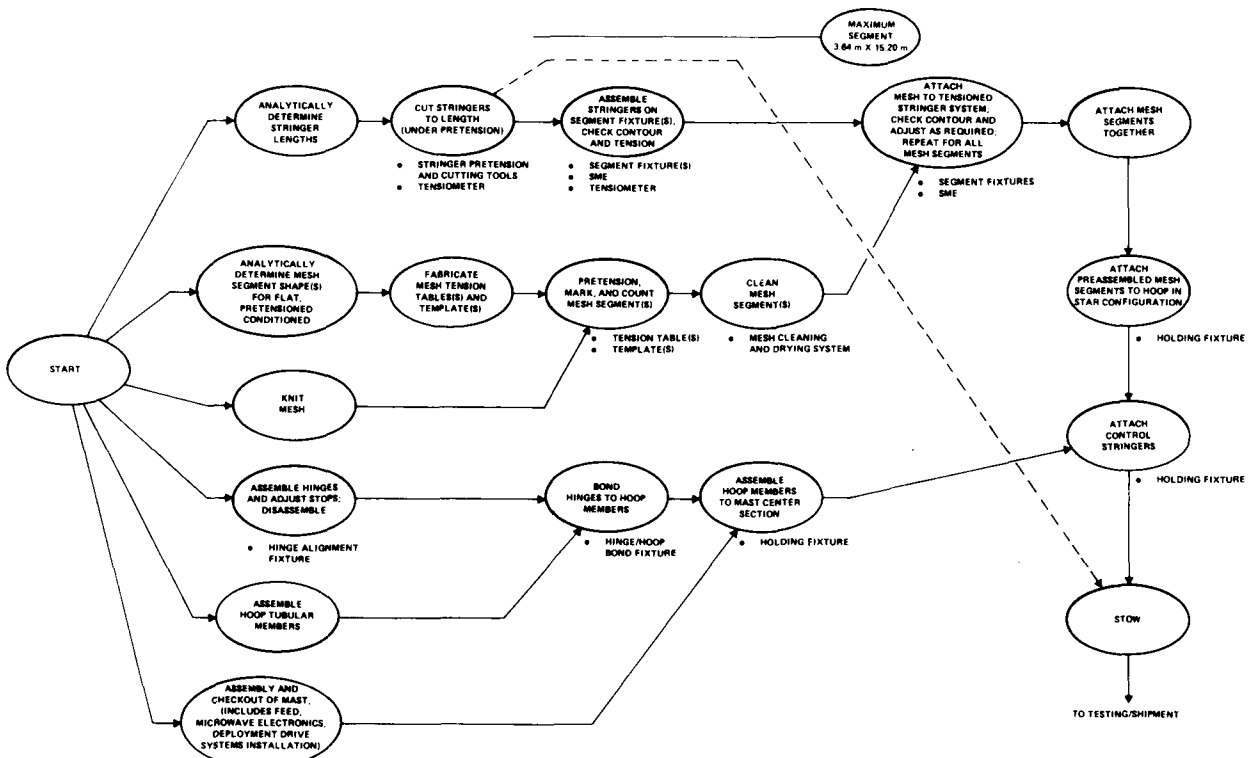


Figure 15. Fabrication Flow Chart

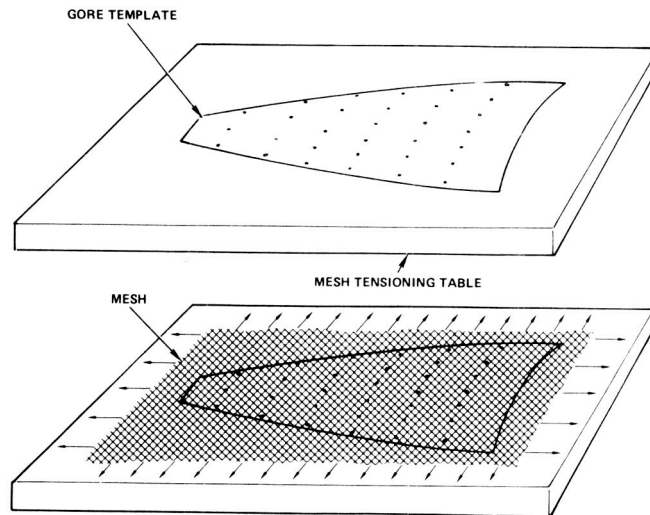


Figure 16. Mesh Tensioning Procedure

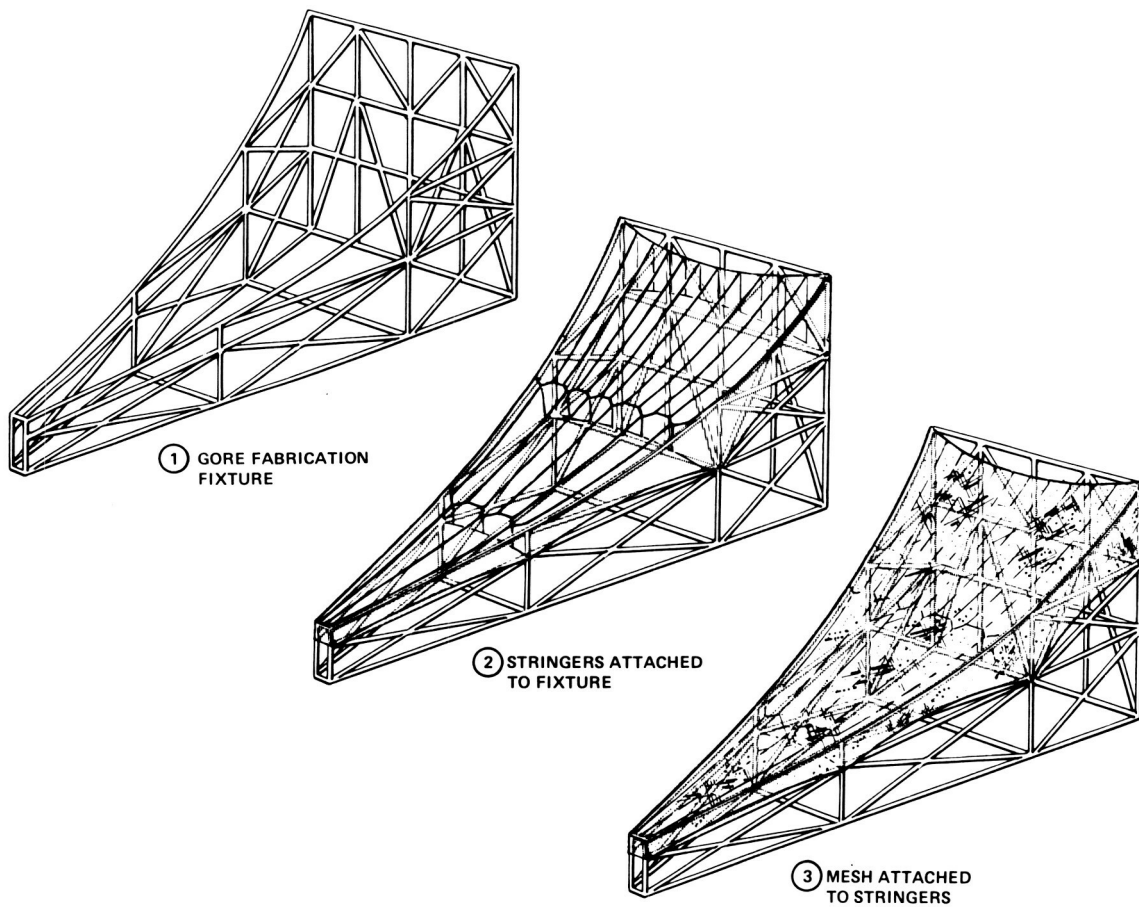


Figure 17. Gore Fabrication Procedure

The tooling used in locating these standoffs is also used for the fixture in which the hoop is assembled. This ensures the accuracy and compatibility of the separate fixtures, and the overall accuracy of the completed antenna.

Intercostals are attached to these standoffs and the stringer-tie skeletal framework assembled. When this arrangement is completed a check of the curvature and location of the elements is made. If adjustments are necessary they are made at this time.

Next, the mesh is placed on the mesh surface stringers, attachments made, and the surface checked again. After completion, this unit is removed from the fixture and set aside for use after all the gore units have been completed. When all of the gore assemblies are completed, they are joined together along their edges to make the complete reflective surface.

Adjacent mesh gores are attached to one another as illustrated in Figure 18, while on the mesh stretch table, quartz tapes are attached to the radial boundaries of the mesh gore by an adhesive. This preserves the mesh tension field. When the gores are attached to the reflector, the adjacent gore edges with quartz tape are sewn together. This technique has been successfully used on smaller deployable reflectors of the rigid radial rib family.

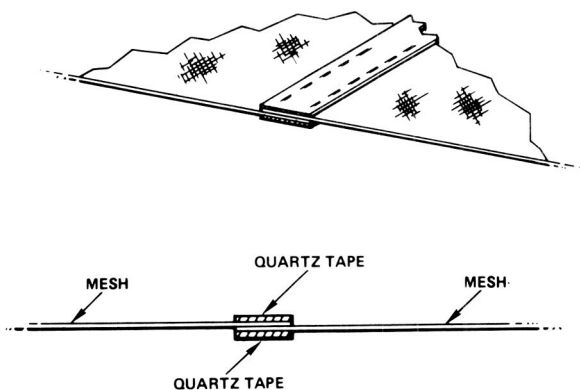


Figure 18. Gore-to-Gore Attachment

The next stage of the assembly sequence is the construction of the hoop. The tubular GFRP members are fabricated to their proper length. The individual hoop segments are then assembled using a fixture to precisely align the tubular GFRP members with the hinges and to ensure the hinges are properly located relative to each other. The fixture is also used as a bonding tool to hold these members in their proper position during the bonding cycle. After the individual segments are completed, they are rechecked prior to installing them in the hoop holding fixture. Once installed in this fixture, the individual hoop segments are joined together, torsion springs put in place, and hinge pins inserted. The mechanical hinge stops are adjusted and locked during this process. This holding fixture is designed to position the completed hoop in the planar star position that it is in after the first stage of hoop deployment.

A separate sequence for fabricating the telescoping mast takes place while the hoop and gore assembly process is underway. The individual GFRP mast sections are fabricated separately and the structural rings that attach at each end of the sections are bonded into position. These rings are machined and match drilled to ensure alignment of adjacent sections when assembled. The hardware, including the Acme threaded rods, sprockets, chains, and motors are all installed and adjusted for proper operation. The spools with the stringers wrapped around them are placed in their retaining brackets located around the mast. All remaining microwave electronics, control system servos and other components are installed and the entire system checked out. Once proper operation is verified, the mast in its stowed configuration is located in position to attach the hoop. This configuration is shown in Figure 19 with the hoop holding fixture not shown for clarity.

At this point, the mesh-secondary drawing surface combination is placed in position around the mast. The intercostals are attached to the hoop hinge joints and the mesh is attached to the proper section of the mast. The stringers are the final components to be attached to the hoop, as shown in Figure 20. Once this is done, the hoop holding fixture is removed and the upper spools containing the stringers which attach to the A joints are driven in reverse. This pulls the A joints up into their final stowed position and the assembly process is completed.

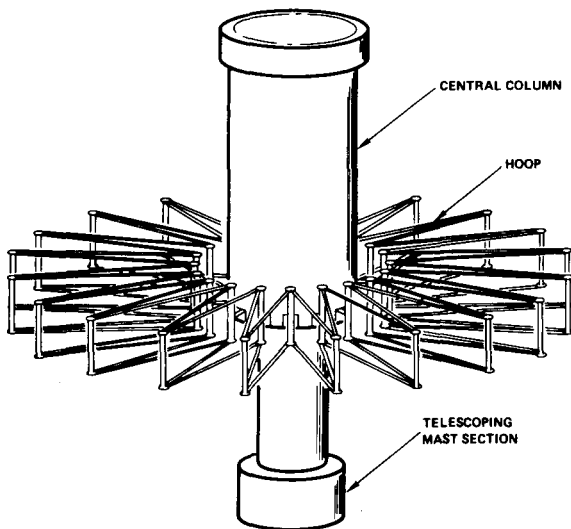


Figure 19. Hoop-to-Central Column
Final Assembly

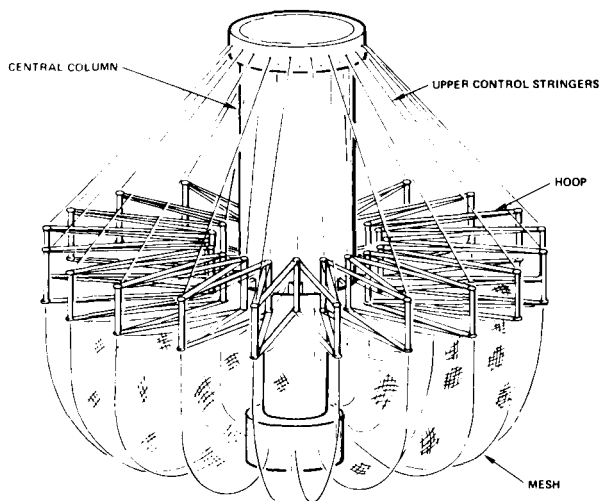


Figure 20. Mesh and Stringer Final Assembly

ENGINEERING MODEL

The engineering model shown in Figure 3 was built to verify the concept feasibility and to aid in uncovering potential design problems. The model was designed with 16 hoop segments and a diameter of 1.82 m. This number of segments was chosen in order to give a realistic assessment of the behavior of the hoop during deployment without complicating the model with additional unnecessary components. There are five separate groups of spools to

which the stringers attach. Two groups are located at the upper position of the mast which control the upper control stringers. One group controls the outer, or A joints, and the other group controls the inner, or B joints. This is required since the inner and outer joints have different rates of deployment. A similar double set arrangement is located at the lower position of the mast to control the lower control stringers attached to the inner and outer joints. The final spool set is located midway up the mast. This set controls the center control stringers which are attached to only the inner joints.

The hoop is made of single aluminum tubular members bonded to aluminum hinge fittings. Since no mesh shaping surface was planned for the model, the double hoop arrangement was not required. The aluminum tube hoop members were slotted lengthwise to allow some torsional compliance. This is required for the final hoop folding operation in the stowing sequence. Because there are only 16 segments the angle of twist of these members is approximately 22 degrees which would have resulted in a shear failure of the tube if the slot was not cut in it.

Torsion springs were designed to deploy the hoop in 1-g, however, the first several attempts at deployment resulted in a significant lowering of the deployment plane. This was caused by the high restraining forces resulting from the weight of the hoop. Figure 21 shows vectorially how these forces increase as the hoop deploys. In order to reduce the restraining component due to the hoop weight, the angle between the upper control stringers and the deployment plane had to increase. This resulted in unsatisfactory deployment and as a result, a zero-gravity fixture was added. This fixture in effect removed the component of the hoop's weight from the upper control stringers and neither aided nor significantly hindered the deployment sequence. The addition of the 0-g fixture allowed the hoop to deploy in the predicted manner.

The model was driven originally by handcranks located on the ends of long shafts beneath the supporting table. These shafts were connected to worm and wheel gearboxes mounted to the underside of the table beneath the mast. The output side of the gearboxes was connected to drive shafts that were connected to the various spools by means of chains and sprockets.

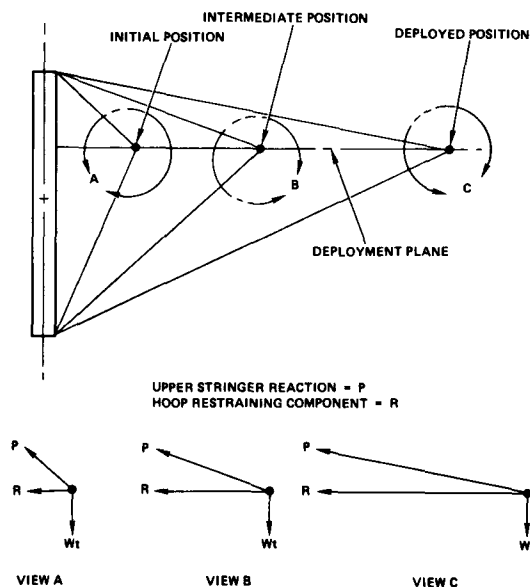


Figure 21. 1-G Loading Deployment Restraining Force

This system was satisfactory but the resulting motion was rather jerky. In an attempt to smooth the sequence, variable speed motors were mounted in place of the handcranks. This addition allowed for a smooth continuous motion deployment which more closely represented the deployment of the actual concept.

Once deployment feasibility was established, a simulated reflective surface was added to the model. A Dacron mesh was cut to the proper shape using the template procedure described for the actual fabrication sequence. The gore elements were sewn together and attached to the mast and hoop. This mesh demonstrated the basic handling and packaging characteristics of the concept.

This model has provided an excellent demonstration of the concept's behavior and has greatly enhanced the confidence in the feasibility of the concept. Specific examples of the concept's behavior which the model exhibited are described below.

The sensitivity of the hoop to control inputs was determined. As the hoop is deployed and all control stringers but the center control stringers are allowed to go slack, no adverse hoop positions occur. However, if the control stringers attached to

the outer joints are in tension and hence restrict deployment causing the center control stringers to go slack, an unfavorable situation can occur. These stringers produce a net force radially inward at each outer joint. This is an unstable situation tending to make the hoop collapse. The stability of the hoop is insured by having the stringers always apply an inward force on the inner joints with little or no net inward force on the outer joints.

If the hoop underwent an undesirable change of shape such as a collapse as a result of such an instability mode, the condition is not catastrophic. The hoop can be restabilized by removing the improper tension from the outer stringers and allowing the hoop to reopen.

The engineering model also showed the importance of mechanical stops at the hinges. The kinematics of the outer joints is such that just prior to full deployment, their motion is reversed. That is, while the joint is increasing its angle, it is actually moving inward towards the mast. If the stops were not present, the joint might conceivably continue inward to a point where it would be impossible to be reversed. This situation would be more prevalent in a 40 joint antenna than in the 16 joint model, since the angle formed between adjacent hoop segments is greater and approaches 180° (157.5° for 16 joints versus 171° for 40 joints).

The engineering model provided valuable insight into the mesh handling characteristics of the concept. The lower control stringers act efficiently as stays which confine the mesh in the stowed position. During the stowing sequence, the mesh must be maintained below the hoop deployment plane to preclude interference or entanglement. This was accomplished by gravity on the engineering model and could be accomplished by the mesh tensioning stringers on orbit. The model has also aided in control system design as well as providing an excellent tool for concept description.

PERFORMANCE PREDICTIONS

Analyses were conducted to determine the performance characteristics of the reflector design as a function of diameter. The following paragraphs present these performance projections.

Weight and Packaging Volume

Table 2 shows the weight breakdown of these antennas. These results are shown graphically in Figure 22. The curves show weight versus antenna diameter and weight per unit aperture area versus antenna diameter. Figure 23 presents packaging volume and packaging density as a function of antenna diameter.

Dynamic Characteristics

The natural frequencies of the stowed antenna were determined using a basic finite element program with the natural frequency of the structure being determined by the Rayleigh method. The results of these analyses are presented in Figures 24 and 25.

Orbital Performance

The analysis flow for the reflector orbital performance is illustrated in Figure 26. The antenna

description (design geometry and material properties) represent, of course, the basic inputs to the various analytical programs. A brief summary of the analysis flow and results follows. A detailed discussion of the modeling is presented in Appendix B.

The NLSA (Non Linear Structural Analysis) program models the mesh surfaces of the antenna using line elements (for intercostals and ties) and triangular membrane elements for the mesh. These are compatible with NASTRAN elements. The output of the program is the equilibrium coordinates of the mesh surface nodes (typically 200 nodes per mesh gore are used) and the stiffness matrix due to the tension in the mesh surfaces. This output is provided to NASTRAN for the determination of the distorted antenna coordinates.

The thermal analysis is performed with the Antenna Thermal Analyzer Program (ATAP). ATAP utilizes the input antenna model characteristics to perform the thermal analysis through the following steps:

Table 2. Weight Budget

	15 m DIA		30 m DIA		100 m DIA	
	LB	kg	LB	kg	LB	kg
HOOP	21	9.5	69	31.3	249	113
HINGES	49	22.2	76	34.5	326	148
STRINGERS AND TIES	16	7.30	68	30.8	621	282
MAST SHELLS AND RINGS	58	26.3	133	60.3	458	208
SPOOLS AND U-JOINTS	43	19.5	84	38.1	279	126
MOTORS, GEAR BOXES AND CLUTCHES	79	35.8	105	47.6	308	140
DRIVE SCREWS	7	3.2	15	6.8	158	72
HARDWARE	27	12.2	34	15.4	96	43
SHROUDS AND BRACKETS	29	13.2	43	19.5	129	58
MESH	16	7.3	64	29.0	509	231
TOTAL W/O FEED EXTENSION MECH.	345	156.5	691	313.3	3133	1421
FEED MAST	33	15.0	62	28.1	241	109
TOTAL	378	172	753	341	3374	1530

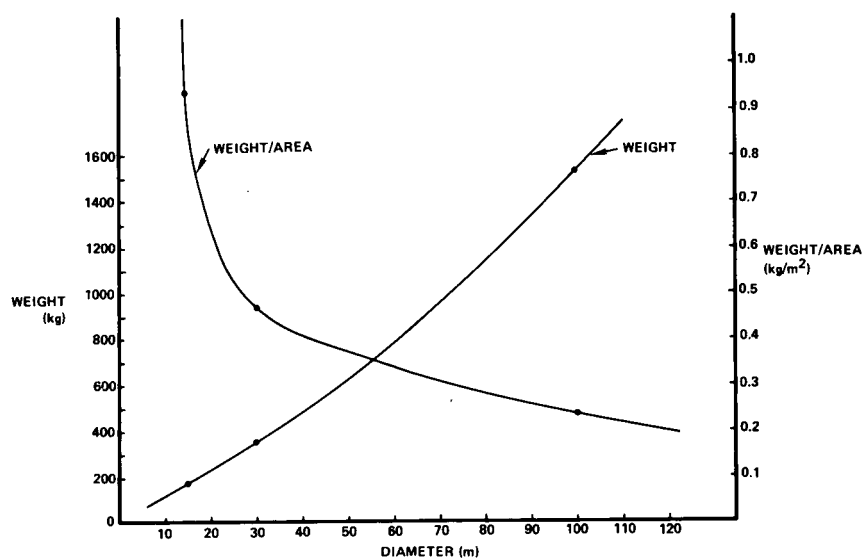


Figure 22. Weight Versus Antenna Diameter

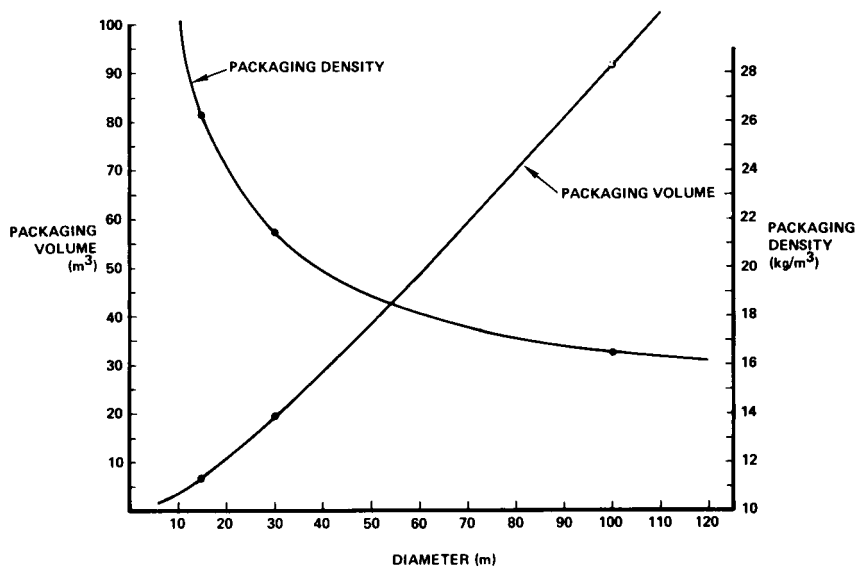


Figure 23. Packaging Volume Versus Antenna Diameter

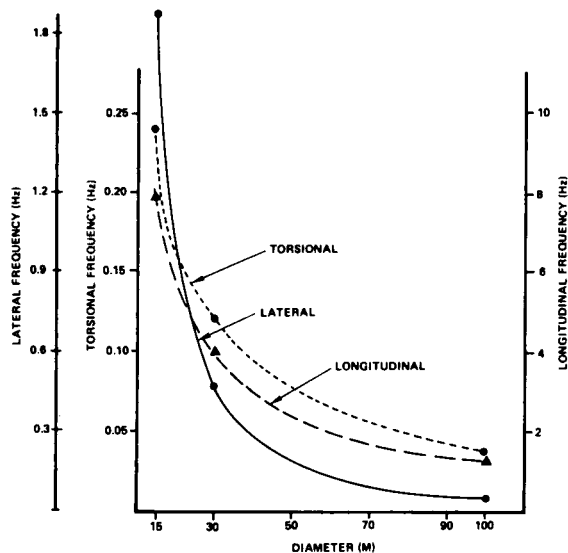
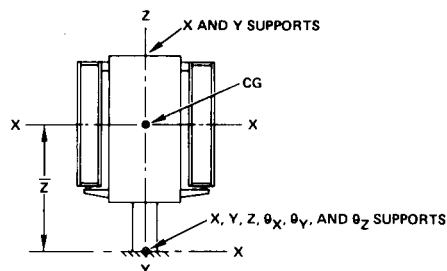


Figure 24. Deployed Dynamic Characteristics



ANTENNA DIAMETER	WEIGHT (kg)	\bar{Z} (m)	I_{xx} (kg-m-SEC ²)	I_z (kg-m-SEC ²)	f_n (Hz)
15 M	172	1.20	6.59	2.71	27.1
30 M	341	1.43	21.10	17.19	11.8
100 M	1,530	3.63	872.3	111.4	3.8

I_{xx} = LONGITUDINAL MASS MOMENT OF INERTIA ABOUT THE CG

I_z = TORSIONAL MASS MOMENT OF INERTIA

f_n = MINIMUM NATURAL FREQUENCY (TORSION ABOUT Z AXIS)

Figure 25. Antenna Stowed Characteristics

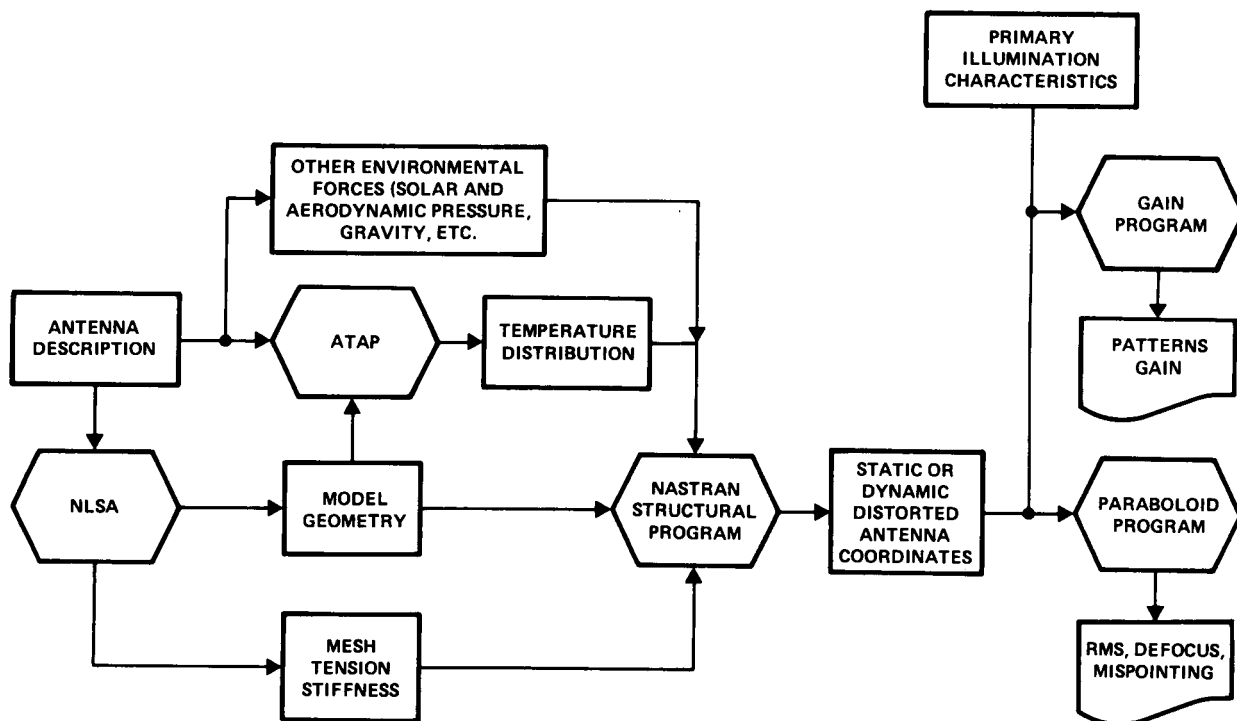


Figure 26. Orbital Performance Analysis Flow

- Generation of the thermal math model including node assignment and distribution.
- Generation of the solar heat flux at the appropriate sun angles. Shadowing effects are accounted for.
- Computes the antenna temperature distribution for steady-state or transient conditions.

The temperature distributions are then provided to the NASTRAN program for the generation of thermal loads.

With the input data from NLSA and ATAP the distorted antenna coordinants are determined. These distorted coordinants and the primary reflector illumination characteristics are provided to the GAIN program. The output of this program are the antenna patterns and gain. For surface contour evaluations, the distorted coordinates are provided to the PARABOLOID program which determines the reflector rms surface error, the axial defocus (from the theoretical focal point), and the mispointing associated with the distorted surface coordinates.

Each of these programs has been previously verified by correlation of analysis predictions with test measurements.

Thermal Distortion

Thermal distortion analyses were performed for two orbital cases. The first case is a 0° sun angle or full solar illumination. The second case is an eclipse condition. The expected component temperature profiles are shown in Table 3. The results of the analyses in terms of defocusing error and surface deviation due to thermal distortions are shown in Table 4 and Figures 27 and 28.

In addition to the thermal distortion analyses described above, limited sensitivity analyses were accomplished to evaluate the impact on surface error due to average temperature of the hoop and differences in temperature between the top and bottom hoop members. The hoop thermal loads are defined by two parameters. One, the average temperature of the hoop and two, the difference in temperature between the top and bottom hoop members. The first load will cause an overall growth

Table 3. Temperature Profiles

$\beta = 0$

COMPONENT	TEMPERATURE		ECLIPSE	
	$^\circ\text{C}$	$^\circ\text{F}$	$^\circ\text{C}$	$^\circ\text{F}$
MESH	221	430	-184	-300
FRONT CORDS	-45	-50	-184	-300
BACK CORDS	-68	-90	-184	-300
INTERCOSTALS	-23	-10	-184	-300
TIES	44	150	-184	-300
HOOP, AVG TEMP	21	70	-54	-65
ΔT FROM TOP TO BOTTOM	55	100	—	—
MAST/TOWER	21	70	21	70

Table 4. Surface Error and Defocus Caused by Thermal Distortion

DIAMETER (METER)	SUN ANGLE = 0				ECLIPSE			
	Δt		RMS		Δt		RMS	
	CM	IN	CM	IN	CM	IN	CM	IN
15	-0.093	-0.037	0.009	0.004	-0.412	-0.162	0.033	0.013
30	-0.189	-0.074	0.019	0.007	-0.814	-0.320	0.066	0.026
100	-0.667	-0.263	0.066	0.026	-2.575	-1.014	0.217	0.085

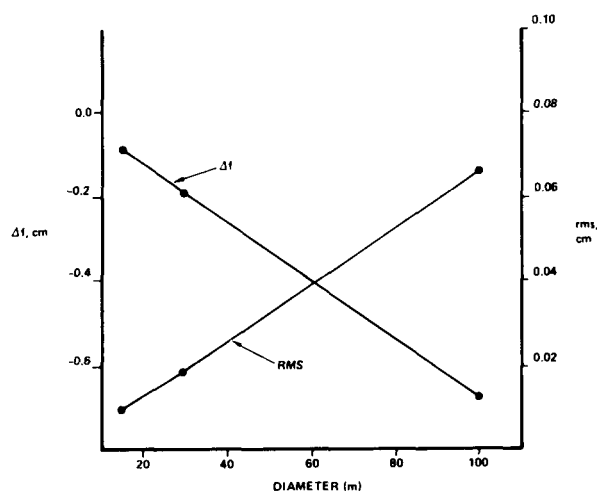


Figure 27. Sun Angle = 0° Thermal Distortion Performance Versus Diameter

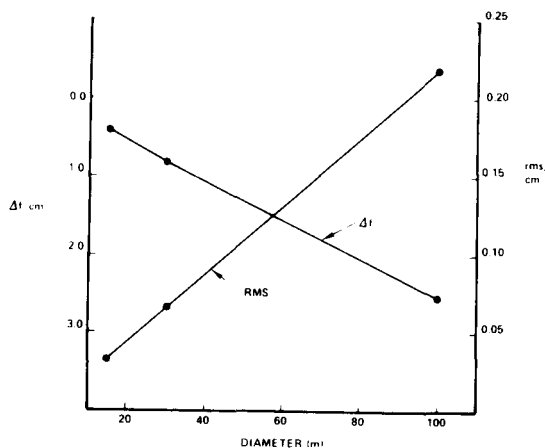


Figure 28. Eclipse Thermal Distortion Performance Versus Diameter

(or shrinkage) of the hoop and the second will cause the hoop to skew due to the top member changing length with respect to the bottom member.

Sensitivities will be obtained by perturbing temperatures about the sun angle = 0 thermal load. For a description of this temperature profile, see the previous section.

The results of the analysis (Figure 29) show very little change in performance over a wide range of temperatures. Thermal devices should provide adequate control of temperatures to maintain the hoop within the bounds of the analysis. Hence, performance will not be impacted.

RF Performance

The major factors associated with reflector gain loss are:

- Blockage — caused by blockage of the aperture by the feed support structure
- Mesh reflectivity
- Surface tolerance
- Defocus effects due to orbital thermal distortions

Each of these loss factors is discussed below. Gain budgets for the 15, 30, and 100 m reflectors

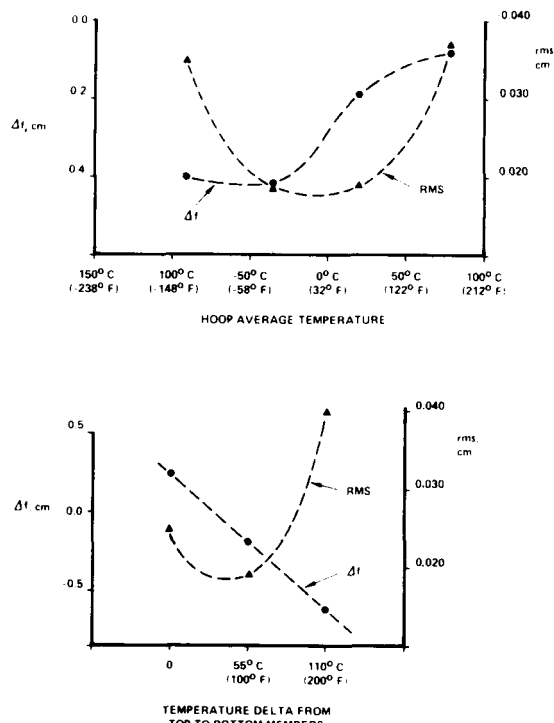


Figure 29. Thermal Distortion Performance for Hoop Temperature Variations at Sun Angle = 0°

are given in Tables 5, 6, and 7. In these gain budgets, a feed efficiency (spillover-amplitude taper) of 75 percent has been arbitrarily assumed.

While a detail study of feed systems for the many potential users (communications, earth observation, RFI detection, radio astronomy, radiometry, etc.) was not undertaken, the reflector design was continuously reviewed to ensure the design did not limit the use of the many possible feed designs (e.g., apex feed systems, Cassegrain feed systems, multiple feeds, etc.). Particular concern was given to the use of multiple feeds since user surveys conducted by both JPL and Langley Research Center indicate the use of multiple feeds in a large percentage of the identified missions.

Because of the large reflector size and hence large feed spacing available, VSWR and the coupling between multiple feeds (each using the complete aperture) induced by the presence of the main reflector and/or subreflector are not a problem as they are with small reflector systems.

Table 5. 15-Meter (49.2 Feet) Diameter Gain Loss Budget

	0.5	1.0	4 GHz	8 GHz
BLOCKAGE	0.13	0.13	0.13	0.13
MESH LOSS	—	0.02	0.06	0.12
*SPILLOVER-TAPER	1.25	1.25	1.25	1.25
SURFACE TOLERANCE	—	0.01	0.12	0.48
AXIAL DEFOCUSING	—	—	0.04	0.18
**MISPOINTING	—	—	—	—
TOTAL LOSS, dB	1.38	1.41	1.60	2.16
GAIN, dB	36.5	42.5	54.3	59.8

*FEED EFFICIENCY OF 75% ASSUMED

**ON-ORBIT CALIBRATION OR AUTOTRACK ASSUMED

Table 6. 30-Meter (98.4 Feet) Diameter Gain Loss Budget

	FREQUENCIES			
	0.5 GHz	1 GHz	2 GHz	4 GHz
BLOCKAGE	0.13	0.13	0.13	0.13
MESH LOSS	0.01	0.02	0.03	0.06
*SPILLOVER-TAPER	1.25	1.25	1.25	1.25
SURFACE TOLERANCE	0.01	0.03	0.10	0.40
AXIAL DEFOCUSING	—	0.01	0.04	0.18
**MISPOINTING	—	—	—	—
TOTAL LOSS, dB	1.40	1.44	1.55	2.02
GAIN, dB	42.5	48.5	54.4	59.9

*FEED EFFICIENCY OF 75% ASSUMED

**AUTOTRACK ASSUMED

Table 7. 100-Meter (328 Feet) Diameter Gain Loss Budget

	0.5 GHz	1 GHz	2 GHz	4 GHz
BLOCKAGE	0.13	0.13	0.13	0.13
MESH LOSS	0.01	0.02	0.03	0.06
*SPILLOVER-TAPER	1.25	1.25	1.25	1.25
SURFACE TOLERANCE	0.06	0.25	1.00	4.02
AXIAL DEFOCUSING	0.03	0.12	0.49	2.03
**MISPOINTING	—	—	—	—
TOTAL LOSS, dB	1.48	1.77	2.90	7.49
GAIN, dB	52.9	58.6	63.5	64.9

*FEED EFFICIENCY OF 75% ASSUMED

**AUTOTRACK ASSUMED

Rudge¹ discusses these problems in detail for a 3.6 m diameter reflector. The magnitude of the effect for a symmetrical Cassegrain system can be calculated using analysis similar to that used by Dragone,² with an adjustment to account for the fact that the capture area of the feed horn is smaller than that of a near-field primary illuminator and the horn-to-subreflector spacing is less. The result is a reflection coefficient or feed-to-feed coupling of -58 dB when a 20 λ subreflector is used. Impacts of this magnitude are negligible for any conceivable application. If apex feeds were used, the effect would be even smaller.

Blockage

Based on design layouts of the reflector designs a maximum aperture blockage of -0.13 dB is projected.

Mesh Reflectivity

The mesh reflectivity losses represent measured test data for the proposed gold-plated molybdenum mesh.

¹Rudge, A. W. et al., "Study of the Performance and Limitations of Multiple-Beam Antennas," Final Report, ESTEC Contract No. 2277/74 HP, Elec. Res. Assoc. (England), Sept. 1975.

²Dragone, C. and D. C. Hogg, "The Radiation Pattern and Impedance of Offset and Symmetrical Near-Field Cassegrainian and Gregorian. IEEE Trans. Antennas and Prop., Vol. AP-22, May 1974, pp. 472-475.

Surface Tolerance and Defocus

The contributors to surface tolerance and defocus losses are given in Tables 8, 9, and 10.

Table 8. 15-Meter Surface Tolerance and Defocus Budget

	$\beta = 0$		ECLIPSE	
	ΔF (mm)	RMS (mm)	ΔF (mm)	RMS (mm)
TIE EFFECTS	—	5.08	—	5.08
MANUFACTURING TOL				
SURFACE SET	—	7.62	—	7.62
MECH ALIGN	± 3.56	—	± 3.56	—
THERMAL EFFECTS				
SURFACE	9.40	1.01	-41.15	3.30
BOOM	2.54	—	2.54	—
TOTAL PREDICTED VALUES	12.45	9.14	43.94	9.65
UNCERTAINTIES				
MATERIAL PROP	43.18	2.29	43.18	2.29
NONREPEATABILITY	63.5	1.78	63.5	1.78
MANUFACTURING	2.79	2.79	2.79	2.79
	77.72	9.91	88.39	10.41

Table 9. 30-Meter Surface Tolerance and Defocus Budget

	$\beta = 0$		ECLIPSE	
	ΔF (mm)	RMS (mm)	ΔF (mm)	RMS (mm)
TIE EFFECTS	—	5.08	—	5.08
MANUFACTURING TOL				
SURFACE SET	—	14.99	—	14.99
MECH ALIGN	± 7.11	—	± 7.11	—
THERMAL EFFECTS				
SURFACE	-19.05	2.03	-82.04	6.60
BOOM	-5.08	—	-5.08	—
TOTAL PREDICTED VALUES	25.15	16.00	87.38	17.02
UNCERTAINTIES				
MATERIAL PROP	86.36	4.57	86.36	4.57
NONREPEATABILITY	127.0	3.56	127.0	3.56
MANUFACTURING	5.59	5.59	5.59	5.59
	155.70	18.03	122.94	18.80

Table 10. 100-Meter Surface Tolerance and Defocus Budget

	$\beta = 0$		ECLIPSE	
	ΔF (mm)	RMS (mm)	ΔF (mm)	RMS (mm)
TIE EFFECTS	—	5.08	—	5.08
MANUFACTURING TOL				
SURFACE SET	—	50.04	—	50.04
MECH ALIGN	23.11	—	23.11	—
THERMAL EFFECTS				
SURFACE	-66.80	6.60	-257.56	21.84
BOOM	-16.51	—	-16.51	—
TOTAL PREDICTED VALUES	86.36	50.8	275.08	54.86
UNCERTAINTIES				
MATERIAL PROP	287.78	15.24	287.78	15.24
NONREPEATABILITY	423.42	11.94	423.42	11.94
MANUFACTURING	18.54	18.54	18.54	18.54
	519.43	57.40	581.41	60.96

The tie effects are caused by a slight dimpling of the mesh at each of the mesh tension tie locations and are a roughness contributor only. The manufacturing tolerance represents engineering judgement of the physical ability to "set" the surface utilizing the adjustable mesh tension ties. The basis for this judgement is experience on four previous reflectors which have utilized the mesh tension tie concept for setting the reflector surface. The mechanical alignment tolerance represents the ability to accurately position the feed system.

The thermal effects are based upon the thermal distortion analyses previously described.

The uncertainty factors included in the budget account for factors which are known to have a statistical variation around a nominal value. These uncertainty factors have been characterized by test and analyses on several previous programs. The material properties uncertainties account for the variation of properties such as coefficient of thermal expansion, modulus of elasticity of the graphite materials, mesh stiffness, etc. The non-repeatability includes diurnal thermoelastic hysteresis and deployment nonrepeatability. The manufacturing uncertainties are those resulting

from the accuracy of surface measurement equipment, uncompensated structural nonlinearity (associated with extrapolating gravity measurements in gravity to zero gravity performance), and uncertainties in the measurement and setting of mechanical alignment.

CONCLUSIONS

This program has met the stated objectives for the feasibility development of the Hoop/Column

concept. This concept satisfies the requirements regarding sizes, multiple deploy and restow capability, weight, reliability and surface accuracy. Feasibility has been demonstrated by means of the 1.82 m diameter engineering model, and analytical predictions show the design capable of obtaining excellent performance. The concept feasibility established during this program forms a solid basis for the full development of the Hoop/Column reflector.

APPENDIX A

CONCEPTS: TRADE-OFF STUDY DESCRIPTION

This section presents the sequence of events leading to the selection of the Hoop/Column concept and briefly describes the major candidate concepts that were considered.

The preliminary design phase began with an investigation of basic deployable antenna categories. Four families of antennas were considered and are shown in Figure A-1. Two of these families were eliminated from further consideration early in the program. The expandable truss family was eliminated because of the large number of mechanisms involved and the known analytical complexity associated with these types of structures. The inflatable family was rejected because of the inherent problems regarding thermal distortion, vulnerability to micrometeorite impact, restowing and weight. It was felt that viable concepts could be developed from both the radial rib and maypole families.

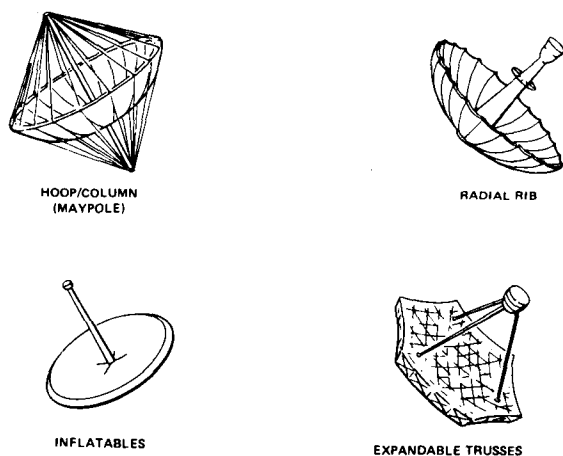


Figure A-1. Concept Families

The first concept considered is called the Articulated Rib concept (see Figure A-2). This concept is the logical extension of Harris ESD's current radial rib design, but has the flexibility to accommodate the diameters under consideration and still retain some packaging efficiency. It consists of a

center mast which supports the feed and to which rigid radial ribs are attached by pivots at the base. Because of the antenna diameters under consideration and the constraint of the limited stowed volume available, it is necessary to put an articulation at the midspan of each rib. The ribs approximate a parabolic contour and have adjustable stand-offs to which the reflective mesh is attached. The surface is shaped between the ribs by the secondary drawing surface technique (see Figure A-3). The concept is attractive from a company experience standpoint, but there are serious packaging size limitations. The shortest stowed length with a single articulation in the ribs is one quarter of the antenna diameter. For a 100 m diameter antenna, this length would become prohibitive. Another articulation for each rib was examined, but the added mechanical complexity and probable mesh handling problems negated the potential advantages.

The second concept considered is also a member of the radial rib family. This design consists of a central hub with multiple astromast* cannisters attached radially around it (see Figure A-4). The feed is also attached to an astromast located in the center of the hub.

Astromasts are articulating lattice structures that are folded into a small volume when stowed and which extend fully when deployed. Deployment takes place by the individual sections of each astromast rib being forced out of its respective cannister. Once fully deployed, the ribs form the desired parabolic shape. The reflective mesh is attached and shaped by the same secondary drawing surface technique used for the articulated rib concept.

The stowed size of this concept is very compact and easily compatible with the shuttle's storage bay. There are, however, serious drawbacks to this concept. The actual attachment of the mesh to the ribs would involve an extremely complex mechanism.

*See waiver on Page 33.

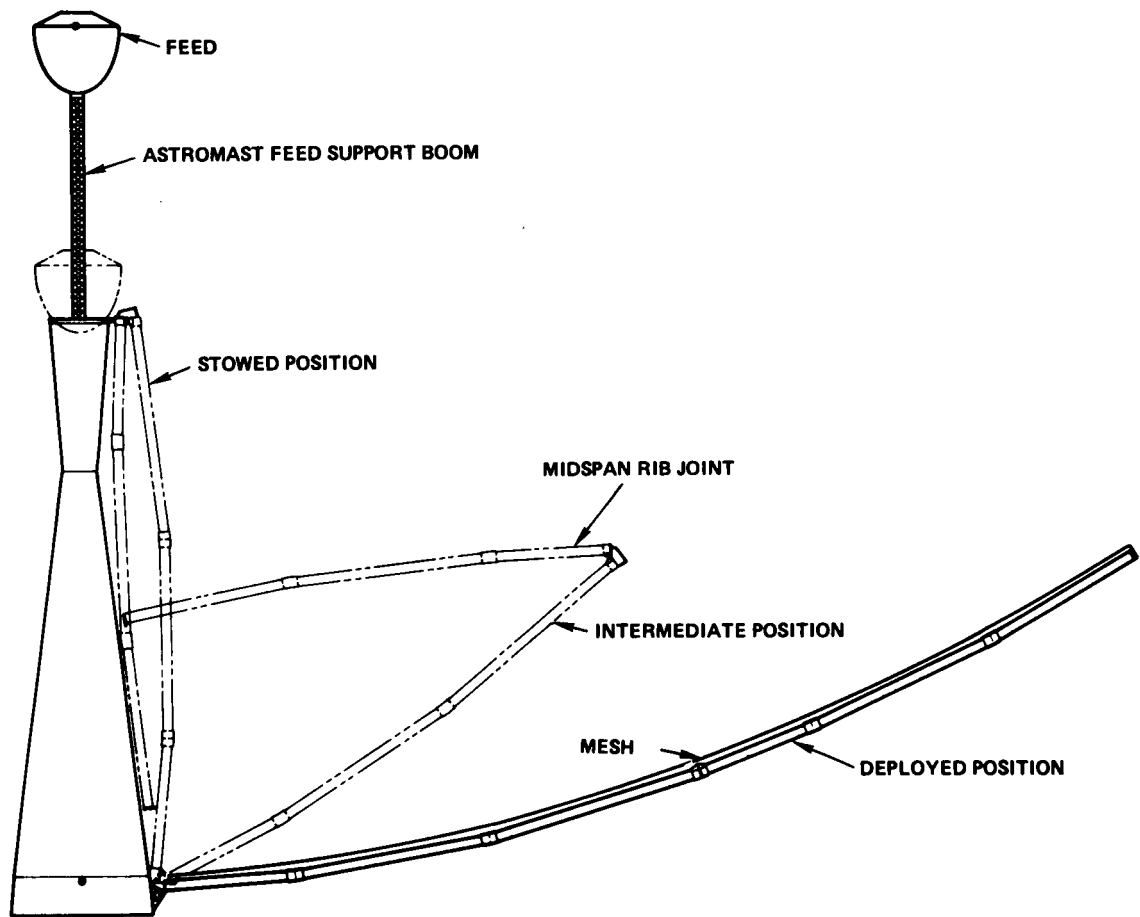


Figure A-2. Articulated Rib Concept

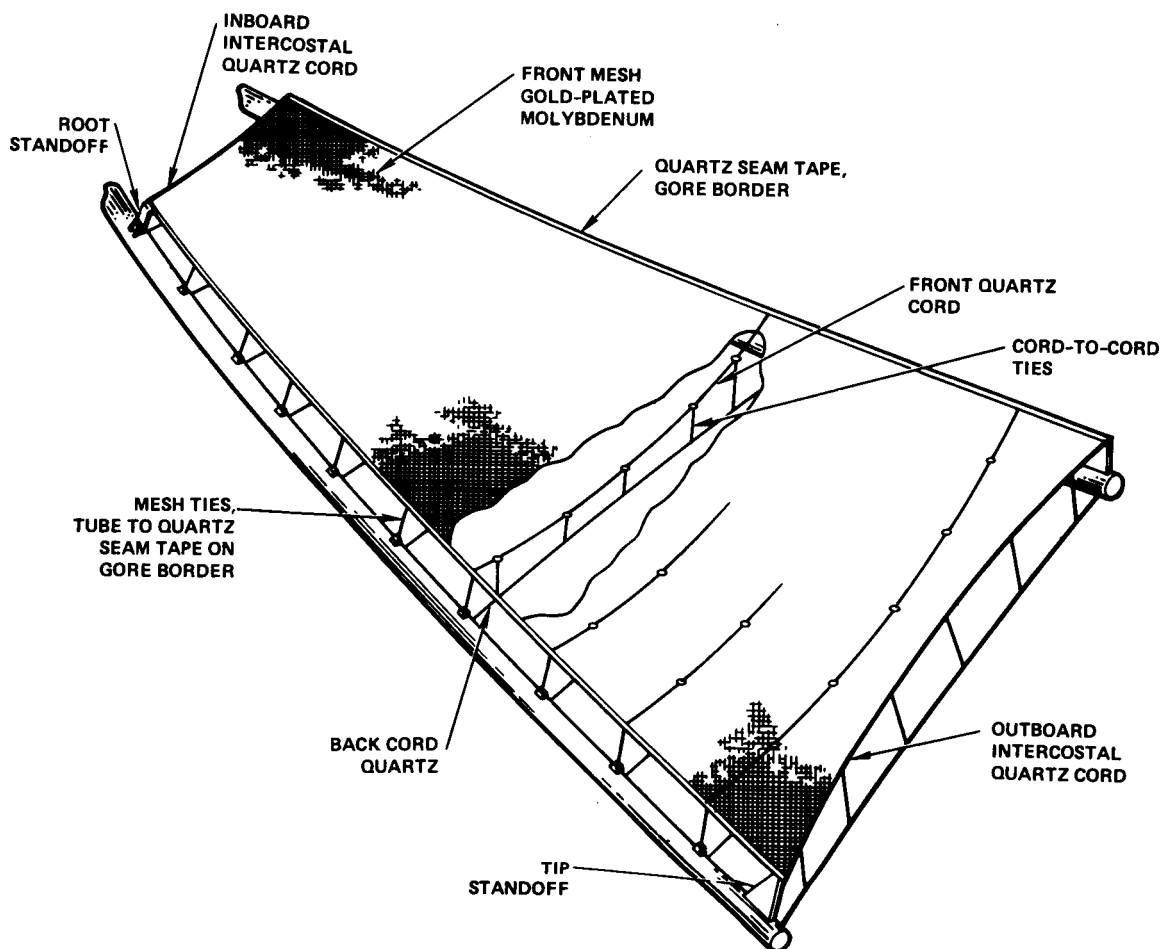


Figure A-3. Secondary Drawing Surface Technique

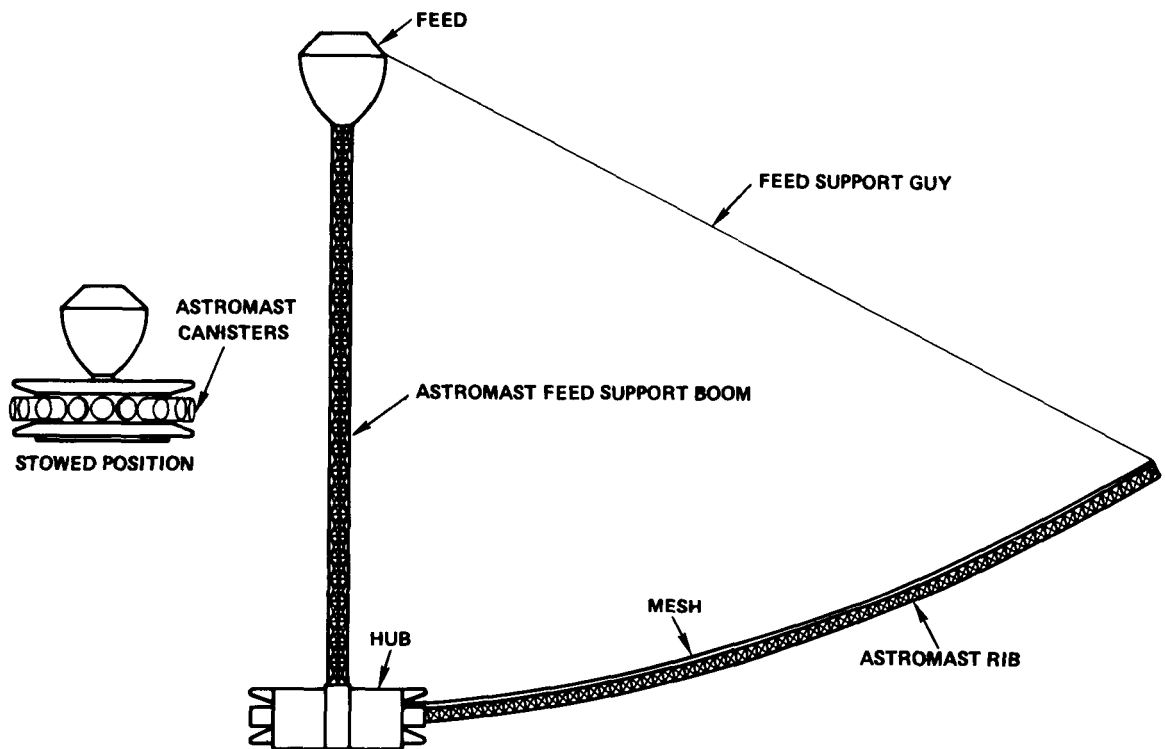


Figure A-4. Curved Astromast Concept

since when stowed the entire astromast is contained within its cannister. The mesh cannot be drawn into this cannister, so it must detach from the ribs as they are being stowed, and reattached upon subsequent deployments. The costs associated with the development of a curved astromast are very high and the additional cost of developing a mechanism capable of attaching and detaching the mesh makes the total cost prohibitive.

The third candidate concept studied was generated as a result of the problems associated with the Curved Astromast concept. The Radial Column concept shown in Figure A-5 eliminates the mesh attachment problem. It employs straight extendable booms which would be either astromasts or some other type of telescoping members. The reflective mesh is not attached along these ribs, but rather to large standoffs at the rib tips. The mesh shaping technique involves the use of a secondary drawing surface similar to the one described for the Hoop/Column concept in the main text. The mesh is supported at its periphery by a series of intercostals which in turn are attached to the tips of the

standoffs. This is shown in Figure A-6. Thus, when the ribs stow, there is no mesh interference problem.

The radial ribs are column loaded due to the mesh and secondary drawing surface loads being reacted by stringers called column preload ties. These ties are attached to the standoffs at their lower end such that no net moment results at the tip of the rib. The inboard end of the rib is attached to the hub by a pin joint which has no moment carrying capability.

This concept is very promising within the majority of the size ranges under consideration. Its potential application near the 100 m size and larger diameters appeared limited however.

The fourth concept investigated was the Hoop/Column concept described in detail in the main text.

After a reasonable effort at optimizing each concept, trade-off studies were performed. The

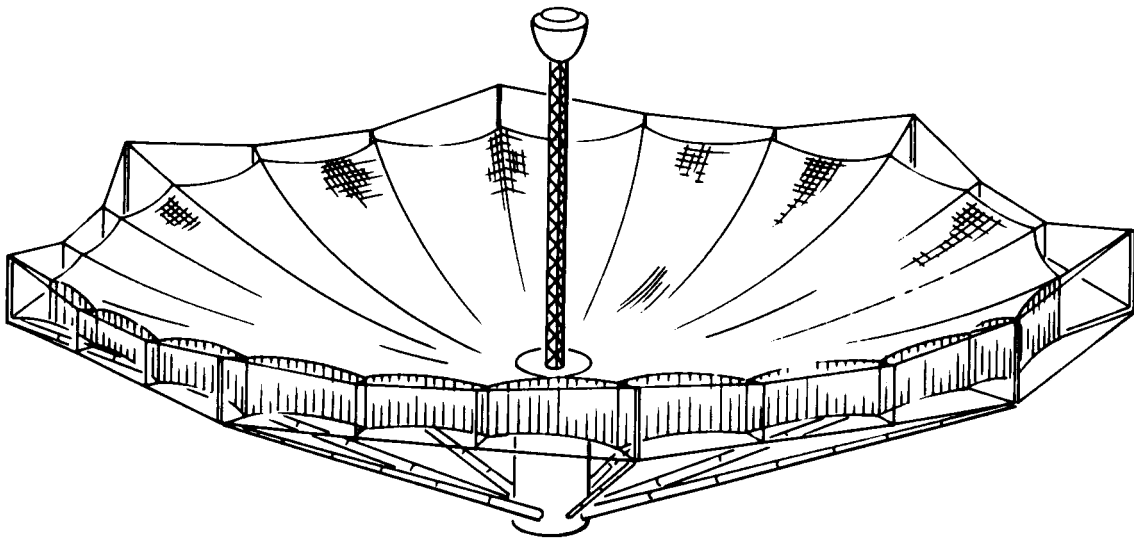


Figure A-5. Radial Column Concept

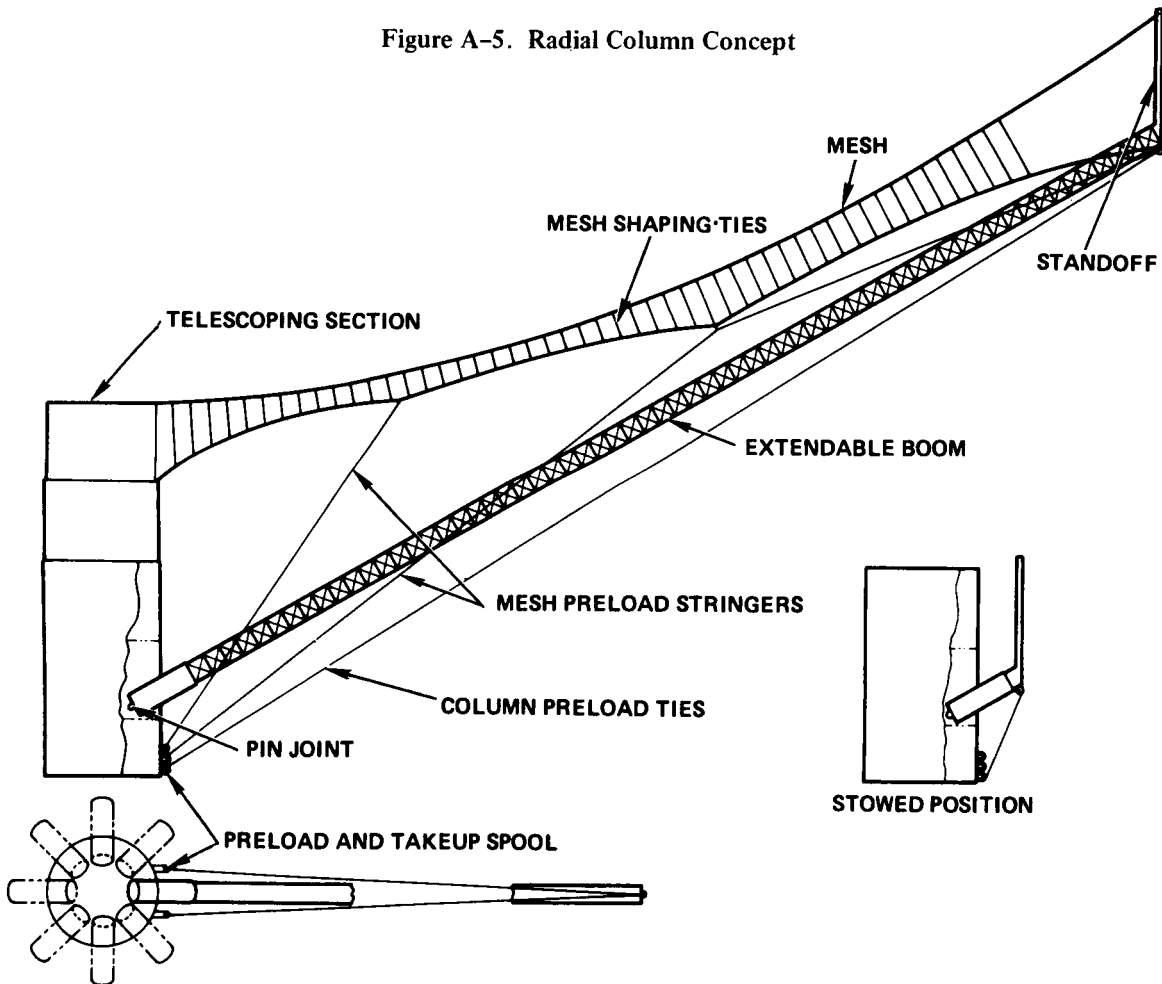


Figure A-6. Radial Column Concept

parameters considered in their relative ranking of importance were as follows:

1. Reliability
2. Surface Accuracy
3. Cost
4. Packaging Volume
5. Weight
6. Dynamic Performance

A list of considerations was generated for each of these categories and each concept was evaluated. These considerations are shown in Figures A-7 through A-9. Where analytical data was available

- CONTROLLED DEPLOYMENT
- NUMBER OF ACTIVE PARTS
- NUMBER OF CRITICAL SERIES OPERATIONS
- MESH HANDLING CHARACTERISTICS
- SIMPLICITY OF CONTROL SYSTEM

Figure A-7. Reliability Considerations

- STRUCTURAL MEMBERS IN TENSION/ COMPRESSION VERSUS BENDING
- EFFECT OF VARYING MESH TENSIONS ON MESH CONTOUR
- USAGE OF LOW CTE MATERIALS
- OPEN STRUCTURE TO MINIMIZE SHADOWING
- NUMBER AND STABILITY OF MESH ATTACHMENT POINTS
- CAPABILITY FOR REMOTE ADJUSTMENT



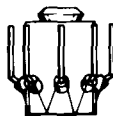

Figure A-8. Surface Accuracy Considerations

- EXTENT OF DEVELOPMENT REQUIRED (NEW TECHNOLOGY VERSUS EXISTING TECHNOLOGY)
- QUANTITY OF HIGH-PRICED MATERIALS REQUIRED
- DESIGN COMPLEXITY
- COMPLEXITY OF MANUFACTURING PROCESS

Figure A-9. Cost Considerations

quantitative comparisons were made. However, in many instances, such as reliability considerations, only qualitative estimates and reasoning could be used. Quantitative results of weight and stowed volume analyses are shown in Figure A-10 for a 30 m diameter antenna.

Figure A-10. Stowed Packaging Volume and Weight for 30-Meter Diameter Antenna

CONCEPT	DIMENSIONS	VOLUME	WEIGHT
 ARTICULATED RIB	3.66 m DIA BY 7.31 m HIGH	75 m ³	563 kg
 CURVED ASTROMAST	3.66 m DIA BY 3.048 m HIGH	32 m ³	458 kg
 RADIAL COLUMN	3.35 m DIA BY 3.96 m HIGH	35 m ³	363 kg
 HOOP/COLUMN	2.5 m DIA BY 3.14 m HIGH	16 m ³	341 kg

The results of these trade-off studies are shown in Figure A-11. The lowest number in this table indicates the best performance under each category.

The overall ranking shows the Hoop/Column concept as being the most capable of meeting the program objectives and it was selected for that reason.

PARAMETER	CURVED ASTROMAST	ARTICULATED RIB	RADIAL COLUMN	HOOP/ COLUMN
RELIABILITY	3	1	2	2
SURFACE ACCURACY	3	3	2	1
COST	4	1	3	2
PACKAGING VOLUME	2	4	3	1
WEIGHT	3	4	2	1
DYNAMIC PERFORMANCE	OK	OK	OK	OK
OVERALL RANKING	4	3	2	1

Figure A-11. Ranking of Concepts

Certain commercial equipment and materials are identified in this paper in order to adequately specify the experimental procedures. In no case does such identification imply recommendation or endorsement of the product by NASA, nor does it imply that the equipment or materials are necessarily the best available for the purpose.

APPENDIX B

ANALYSIS

Model Description

To predict performance of the concept, the 30 m antenna was modelled as shown in Figure B-1. The model is only half a gore. This is all that is necessary to analyze symmetric loads. Since the concept uses nonlinear elements with pretensions, the model employs a proprietary finite element Nonlinear Structure Analysis Program, NLSA. NLSA handles both pretension stiffness and geometric nonlinearity.

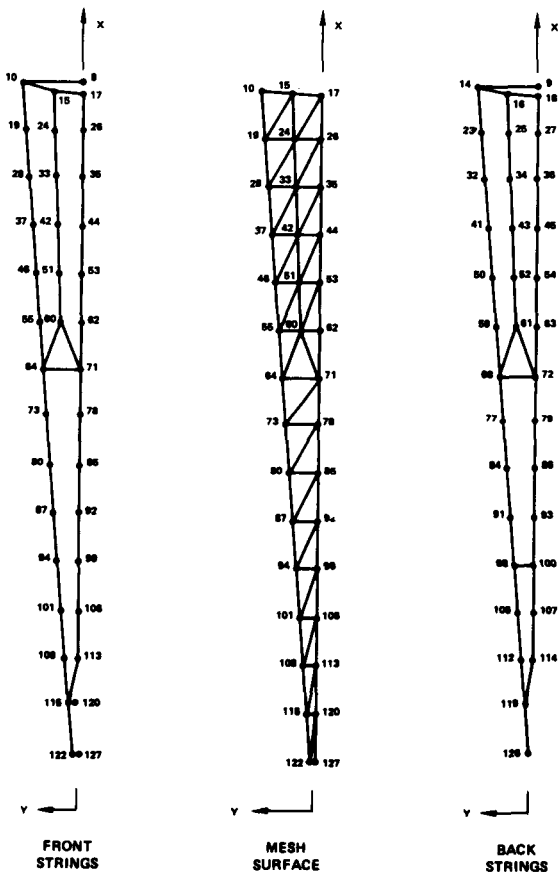


Figure B-1. Half-Gore Model

The model consists of one-hundred fourteen string type elements, thirty-nine membrane elements and three beam elements in the configuration shown in Figures B-1 and B-2. Members and pretensions are sized to be compatible with the concept as designed. Note that some condensation has been done in that one model cord represents one and a half design cords.

Component Description

Design values of pretensions are predicated on the tension in the mesh and front cords. To maintain cord dominance of the structure, front cord tension should be on the order of five to ten times the mesh tension in the direction of the cords, times the cord spacing.

$$T_c = 5 T_m S_c$$

The tensions are required to also maintain the cords in the linear range of the load deflection curve and provide adequate margin for breakage. A typical curve is shown in Figure B-3. The curve is for a five stranded cord. The operational load per strand is $(2.94 \text{ NT}/5) = 0.6 \text{ NT}$. Once the cord tension as required by the design is found, the number of strands needed is the cord tension divided by 0.6.

Mesh tensions are $0.035 \text{ NT}/\text{CM} \times 0.0175 \text{ NT}/\text{CM}$ ($0.020 \times 0.010 \text{ lb}/\text{in.}$) in the circumferential and radial directions. Since cords run radially, their tensions are $0.0875 \text{ NT}/\text{CM}$ times the spacing. The spacing is related to the allowable surface error due to mesh bulge. Mesh bulge is a result of the tension and doubly curved surface. Analytic results indicate that the RMS of the bulge for the 30 m dish with a cord spacing of 40 CM ($\sim 16 \text{ in.}$) is 0.051 CM (0.020 in.). See the section on surface approximations for details. With this spacing, front cord tension is 3.50 NT. The number of strands per cord is six.

Knowing front surface tensions, the back cord tensions can be determined. The back cords must provide the forces to hold the front surface in the

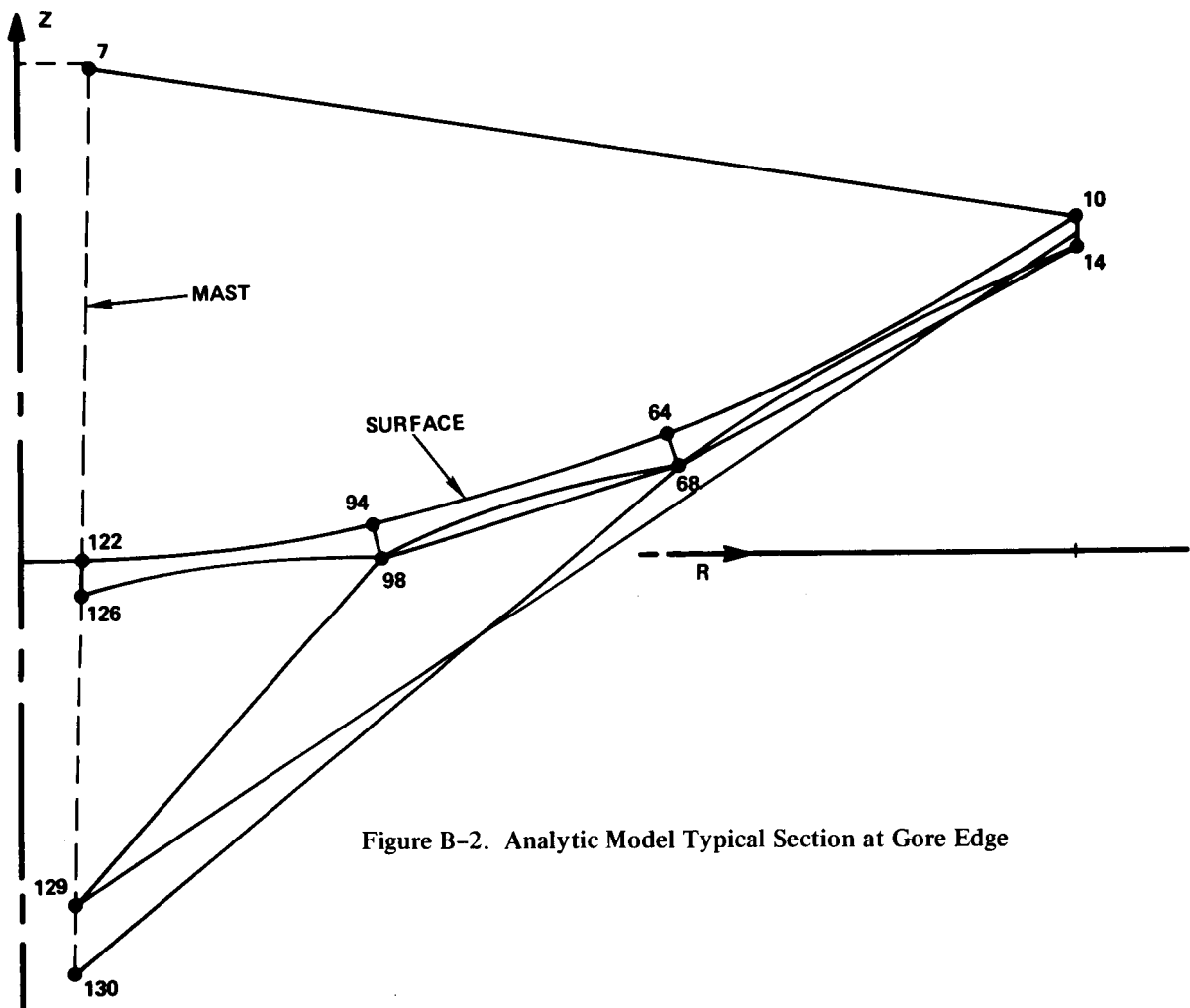


Figure B-2. Analytic Model Typical Section at Gore Edge

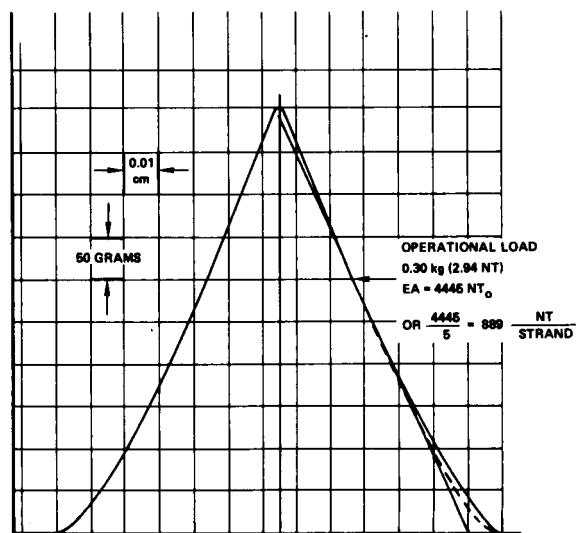


Figure B-3. Load Deflection of 5-Stranded Cord

shape of a parabola. The tension in these cords now becomes a function of geometry, mainly the amount of arch in the back cords. A trade-off between back cord tension, arch and tie length becomes apparent. The larger the arch, the shorter the ties. Too little arch will require much cord tension and, therefore, high hoop loads. Experience has shown that tie lengths less than 5.0 cm (2 inches) become too hard to adjust. Therefore, a tie length of 7.5 cm (3 inches) was established as a minimum design value. This allows for adequate adjustment margin and makes for easier handling.

Maximum tie lengths are constrained by packaging considerations and back stringer geometries. Examination of Figure B-2 will illustrate the geometry considerations. As tie 64-68 becomes longer, the effectiveness of back stringer 130-68-14 in holding the surface in the desired shape is weakened. As a result, the stringer load must also increase. This leads to an undesirable increase in hoop load.

The result of several attempts at sizing back cord loads was a pretension in the back cords of 7.0 NT (1.57 lb). This tension level yielded minimum tie lengths of 8.5 cm (3.5 in.).

The preloads for the other components are then found through the equilibrium equations for each node in the model. These preloads are listed in Table B-1.

Cord Spacing — Surface Approximations

Due to the pretensions in the mesh and surface curvature, the mesh between cords bulges up. This bulging causes a surface distortion and contributes to the RMS of the system. The amount of this distortion is a function of cord spacing. A derivation of the RMS as a function of this spacing follows. The output of the derivation defines the cord spacing required to meet a given RMS. Analytical results confirm the derivation.

The pillow can be viewed as a one-dimensional bulge between parallel cords. Under this assumption, one can employ the equation of a string under uniform load. Using membrane theory, it can be shown that at the center of the gore, the equivalent pressure is:

Table B-1. Design Summary

MESH

GOLD-PLATED 1.2 MIL (0.030 CM) DIAMETER MOLYBDENUM WIRE
OPERATING TENSIONS OF 0.035 X 0.0175 NT/CM (0.02 X 0.010 LB/IN.),
CIRCUMFERENTIAL AND RADIAL DIRECTIONS.

STIFFNESS (NT/CM):

$$\begin{bmatrix} N_x \\ N_y \\ N_{xy} \end{bmatrix} = \begin{bmatrix} 0.90 & 1.12 & 0 \\ 1.12 & 1.69 & 0 \\ 0 & 0 & 0.61 \end{bmatrix} \begin{bmatrix} E_x \\ E_y \\ E_{xy} \end{bmatrix} + \begin{bmatrix} 0.035 & -\alpha T \\ 0.0175 & -\alpha T \\ 0 & 0 \end{bmatrix}$$

α , THERMAL COEFFICIENT OF EXPANSION IS

$5.4 \times 10^{-6}/^{\circ}\text{C}$ ($3.0 \times 10^{-6}/^{\circ}\text{F}$) AT ROOM TEMPERATURE

MASS, $2.3 \times 10^{-6} \text{ kg/CM}^2$ ($3.3 \times 10^{-5} \text{ LB/IN.}^2$)

CORD STRANDS

QUARTZ FIBERS, EACH STRAND MADE OF 220 FIBERS.

OPERATING TENSION PER STRAND, 0.6 NT (OR 0.13 LB)

STIFFNESS, $E_A = 889 \text{ NT}$ (200 LB)

BREAKING STRENGTH, 6.7 NT (1.5 LB)

α , CTE, $0.54 \times 10^{-6}/^{\circ}\text{C}$ ($0.3 \times 10^{-6}/^{\circ}\text{F}$) AT ROOM TEMPERATURE

MASS, $2.0 \times 10^{-6} \text{ kg/CM}$ ($1.1 \times 10^{-5} \text{ LB/IN.}$)

HOOP

GRAPHITE/EPOXY, LAYUP (0, 90, ± 45)

$E = 0.89 \times 10^7 \text{ NT/CM}^2$ (10^7 PSI)

$G = 0.27 \times 10^7 \text{ NT/CM}^2$ ($4 \times 10^6 \text{ PSI}$)

α , CTE, $0.81 \times 10^{-6}/^{\circ}\text{C}$ ($0.45 \times 10^{-6}/^{\circ}\text{F}$) AT ROOM TEMPERATURE

MASS, $1.6 \times 10^{-3} \text{ kg/CM}^3$ (0.06 LB/IN.^3)

TOP MEMBER, 5.08 CM X 0.051 CM TUBE (2.0 IN. X 0.20 IN.)

$A = 0.811 \text{ CM}^2$

$I = 2.626 \text{ CM}^4$ COMPRESSIVE PRELOAD: 3011 NT = 677 LBS

$J = 5.251 \text{ CM}^4$

BOTTOM MEMBER, 5.08 CM X 0.030 CM TUBE (2.0 IN. X 0.012 IN.)

$A = 0.486 \text{ CM}^2$

$I = 1.544 \text{ CM}^4$ COMPRESSIVE PRELOAD: 755 NT = 170 LBS

$J = 3.089 \text{ CM}^4$

CROSS LINK, 5.72 CM X 0.318 CM TUBE (2.24 IN. X 0.125 IN.)

$A = 5.7 \text{ CM}^2$

$I = 23.31 \text{ CM}^4$ TENSILE PRELOAD: 27 NT = 6 LBS

$J = 46.62 \text{ CM}^4$

CORDS

COMPONENT	STRANDS	TENSION		NT	EA (LB)
		NT	(LB)		
FRONT (SURFACE)	6	3.5	0.79	5,334	(1,200)
BACK (SURFACE)	12	7.0	1.57	10,668	(2,400)
UPPER STRINGER	800	454	102	6.7×10^5	(1.5×10^5)
LOWER STRINGERS*					
(14-68)	140	84		1.2×10^5	(2.8×10^4)
(68-130)	150	92		1.4×10^5	(3.1×10^4)
(68-98)	160	94		1.4×10^5	(3.1×10^4)
(98-129)	170	104		1.5×10^5	(3.5×10^4)
INTERCOSTALS					
FRONT	25	15		2.2×10^4	(5,000)
BACK	67	40		5.9×10^4	(1.3×10^4)

* (N-M) REFERS TO MODEL NODE NUMBERS

$$P = \frac{1}{2f} \left[N_C \cos \theta + N_R \cos^3 \theta \right]$$

where f = focal length

N_C = mesh traverse tension

N_R = mesh meridional tension

θ = $\tan^{-1} (r/2f)$

r = radius

Apply the string equation to a strip of mesh between the cords of spacing s ,

$$d_t = \frac{1}{\cos \theta} \frac{P s^2}{8 N_c}$$

This is the contribution from surface tension to the pillow height. Another contribution comes from geometry of the parabola. Its value is:

$$d_g = \frac{s^2}{16f}$$

The total pillow height is then $d_t + d_g$. Previous analysis has shown that the RMS of the pillow is approximately 1/4 of the pillow height. Therefore:

$$s = \sqrt{\frac{4* (\text{RMS})}{\frac{1}{16f} + \frac{1}{\cos \theta} \frac{p}{8N_c}}}$$

Using this relation, cord spacing required to meet a specified RMS is defined. This relation was employed to define cord spacing. To project on-orbit performance, a model was generated and analysis performed. The model is depicted in Figures B-4 and B-5. Results of the analyses are shown in Table B-2.

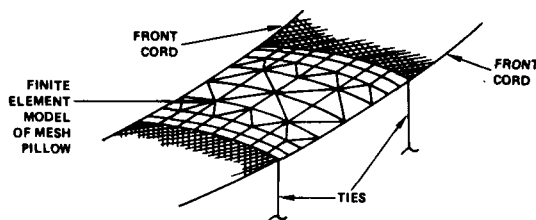


Figure B-4. Pillows Model to Determine Mesh Bulge

Thermoelastic Predictions

Temperature Profiles

The expected component temperatures for the 0° sun angle are summarized below:

Component	Temperature	
	°C	°F
Mesh	221	430
Front Cords	-45	-50
Back Cords	-68	-90
Intercostals	-23	-10
Ties	44	150
Hoop, Ave. Temp	21	70
ΔT from Top to Bottom	55	100
Mast/Tower	21	70

As a design goal, the average hoop temperature will be 21° C (70° F). However, during head-on sun, the differential temperature between top and bottom members could be large, hence the choice of 55° C. Likewise for the mast, except that better thermal controls will limit development of gradients.

For the eclipse condition, the profile is:

	°C	°F
Mesh	-184	-300
Cords, Front and Back	-184	-300
Intercostals	-184	-300
Ties	-184	-300
Hoop	-54	-65
Tower/Mast	21	70

As depicted in Figure B-6, the CTE of quartz changes with temperature. To take this into account in the T/E analysis, tables of thermal strains will be calculated based upon the following:

$$I(t) = \int_{T=20^{\circ}\text{C}}^{T=T} \alpha(T) dT$$

Results of tests run on quartz cords with the same construction as proposed are pictured in Figure B-7. Based upon this data, $I(t)$ for the cords is shown in Table B-3.

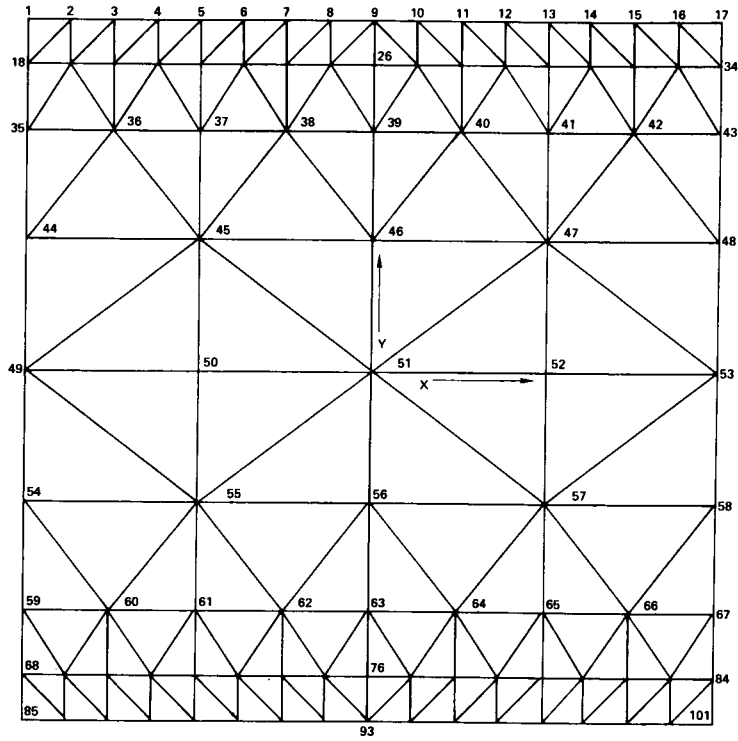


Figure B-5. Pillow Model Nodes 1, 17, 85, 101 Are T/E Points

Table B-2. Pillow Bulge, T/E Effects

DIAMETER	CORD AND TIE SPACING	NOMINAL		AT 230° C (430° F)		AT -184° C (-300° F)	
		PEAK	RMS	PEAK	RMS	PEAK	RMS
30M	40 X 40 CM	0.212 CM	0.052 CM	0.209 CM	0.051 CM	0.220 CM	0.053 CM
100M	70 X 70 CM	0.211 CM	0.049 CM	0.208 CM	0.049 CM	0.216 CM	0.050 CM
15M	25 X 25 CM	0.150 CM	0.038 CM	0.148 CM	0.037 CM	0.154 CM	0.038 CM

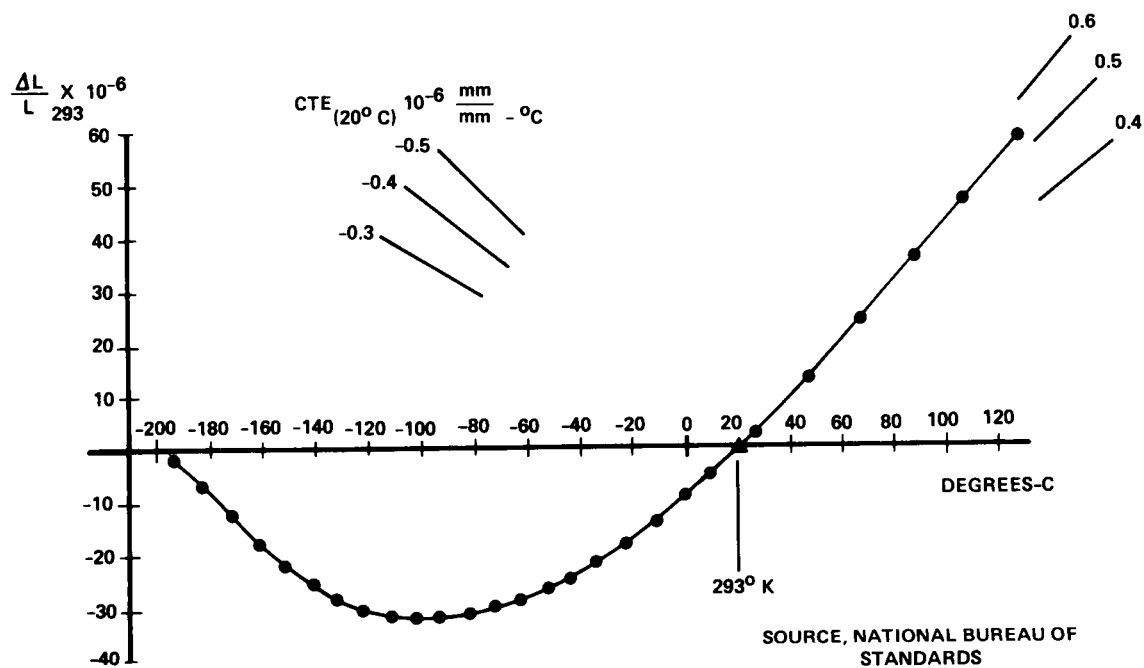


Figure B-6. Thermal Expansion of Quartz Versus Temperature

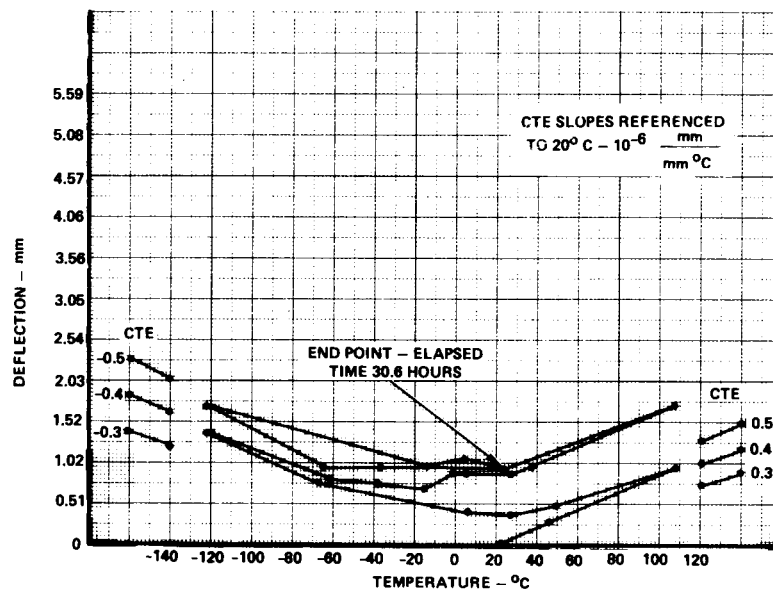


Figure B-7. Cord Thermal Expansion Test

Table B-3. Front and Rear Cords

FRONT AND REAR CORDS			TIES		
T, °C	°F	I (T) X 10 ⁶	T, °C	°F	I (T) X 10 ⁶
-240	-400	72.65	21	70	0
+184	-300	48.65	149	300	450.8
-129	-200	24.65	260	500	842.8
-65	-85	-2.95	-18	0	-70.7
-18	0	-1.33	-129	-200	-272.7
21	70	0.0	-240	-400	-474.7
38	100	6.1			
93	200	30.1			
149	300	54.1			
204	400	78.1			
260	500	102.1			

INTERCOSTALS			MESH		
T, °C	°F	I (T) X 10 ⁶	T, °C	°F	I (T) X 10 ⁶
-240	-400	41.5	-273	-460	-956.6
-184	-300	17.5	-226	-374	-935.1
-129	-200	-6.5	-198	-324	-896.1
-73	-100	-30.5	-173	-279	-838.45
-65	-85	-34.1	-123	-89	-671.05
-18	0	-15.4	-73	-99.4	-455.95
21	70	0.0	-23	-9.4	-218.35
93	200	53.3	21	70.0	0.0
149	300	94.3	77	170.6	282.1
204	400	135.3	127	260.6	539.5
			227	440.6	1064.2
			327	620.6	1598.8
			427	800.6	2144.2

FOR THE GRAPHITE HOOP MEMBERS, A CONSTANT VALUE OF α_{CTE} IS ASSUMED, ITS VALUE $0.81 \times 10^{-6}/^{\circ}\text{C}$ ($0.45 \times 10^{-6}/^{\circ}\text{F}$).
FROM THE ABOVE TABLES, VALUES OF I (T) FOR ALL ELEMENTS CAN BE FOUND AND INPUTTED TO THE THERMOELASTIC ANALYSIS.

Results of Thermoelastic Analyses

Performance of the 15, 30 and 100 m antennas are summarized in Table B-4.

Table B-4. Antenna Performance

DIAMETER (METER)	SUN ANGLE = 0				ECLIPSE			
	Δt		RMS		Δt		RMS	
	CM	IN	CM	IN	CM	IN	CM	IN
15	-0.093	-0.037	0.009	0.004	-0.412	-0.162	0.033	0.013
30	-0.189	-0.074	0.019	0.007	-0.814	-0.320	0.066	0.026
100	-0.667	-0.263	0.066	0.026	-2.575	-1.014	0.217	0.085

Geographical results are depicted in Figures B-8 and B-9.

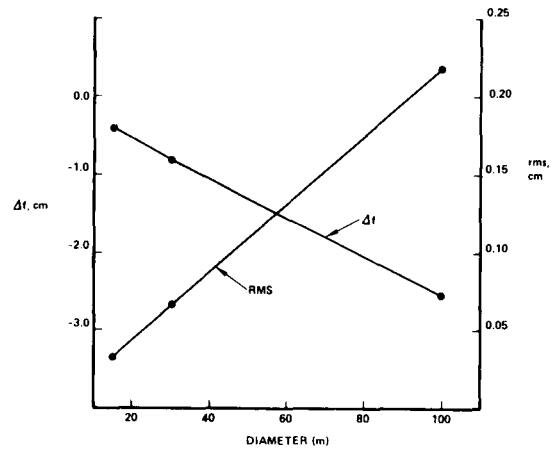


Figure B-8. Eclipse Performance Versus Diameter

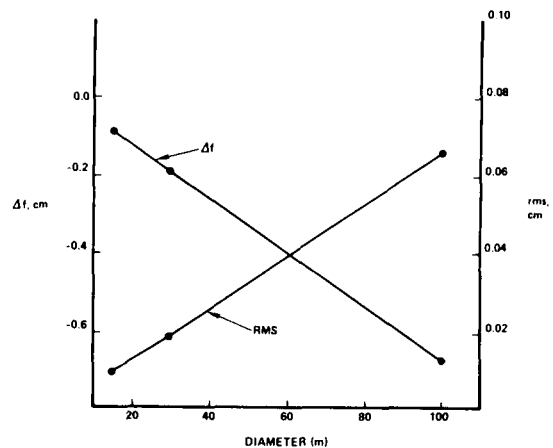


Figure B-9. Sun Angle = 0 Performance Versus Diameter

Hoop Temperature Sensitivity

The hoop thermal loads are defined by two parameters. One, the average temperature of the hoop, and two, the difference in temperature between the top and bottom hoop members. The first load will cause an overall growth (or shrinkage) of the hoop and the second will cause the hoop to skew due to the top member changing length with respect to the bottom member.

Sensitivities will be obtained by perturbing temperatures about the sun angle = 0 thermal load. For a description of this temperature profile, see the previous section.

The results of the analysis, Figure B-10, show very little change in performance over a wide range of temperatures. Thermal devices should provide adequate control of temperatures to maintain the hoop within the bounds of the analysis. Hence, performance will not be impacted.

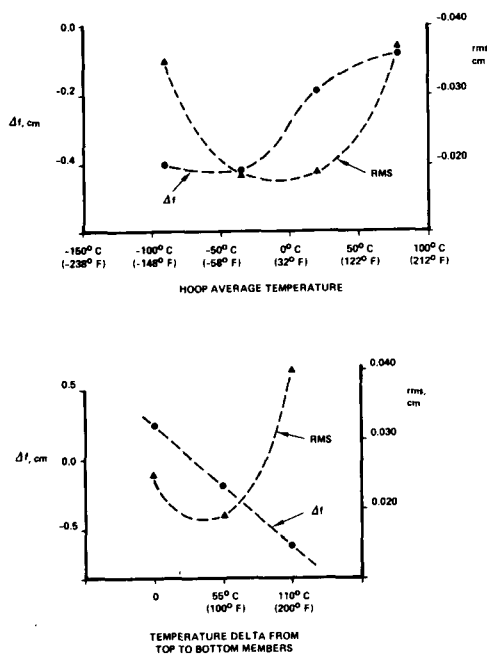
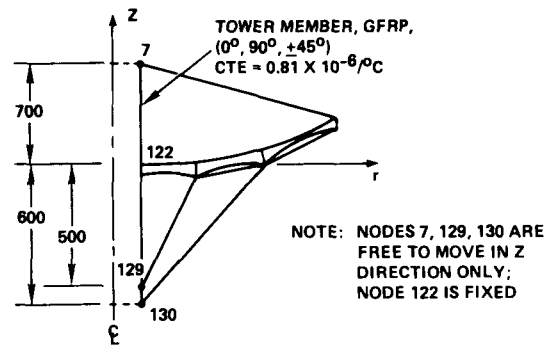


Figure B-10. Performance for Hoop Temperature Variations at Sun Angle = 0 30-Meter Diameter

Tower T/E Effects

To investigate tower T/E effects, an analysis was run using the $B = 0$ temperature profile. Tower T/E effects are introduced by thermally loading members to simulate tower expansion.



Since Node 7 is in the sun at $B = 0$, and Nodes 129, 130 are not, the following profile for temperature changes is assumed.

NODE	ΔT
7	+55° C (100° F)
130	-55° C (-100° F)
122	$55 - \frac{700}{1300} 110 = -4.23° C (-8° F)$
129	$55 - \frac{1200}{1300} 110 = -46.54° C (-84° F)$

NOTE: Linear variation in ΔT from Node 7 to Node 130 assumed.

Results for Tower T/E:

$$\Delta f = 0.244 \text{ cm}$$

$$\text{RMS} = 0.022 \text{ cm}$$

For comparison, at $B = 0$ with quiescent tower,

$$\Delta f = 0.189 \text{ cm}$$

$$\text{RMS} = 0.019 \text{ cm}$$

The tower temperature profile used in the above is extreme with the gradient from front to back being 110° C (200° F). Thermal controls will lessen this gradient. Therefore, it is apparent from the results that tower effects on the surface are small.

1. Report No. CR-2894		2. Government Accession No.		3. Recipient's Catalog No.	
4. Title and Subtitle AAFE Large Deployable Antenna Development Program - Executive Summary				5. Report Date October 1977	
				6. Performing Organization Code	
7. Author(s)				8. Performing Organization Report No.	
				10. Work Unit No.	
9. Performing Organization Name and Address Harris Corporation Melbourne, Florida				11. Contract or Grant No. NAS1-13943	
				13. Type of Report and Period Covered Contractor Report	
12. Sponsoring Agency Name and Address National Aeronautics & Space Administration Washington, DC 20546				14. Sponsoring Agency Code	
15. Supplementary Notes Langley Technical Monitor: Thomas G. Campbell Final Report					
16. Abstract This report describes the Large Deployable Antenna Development Program sponsored by the Advanced Applications Flight Experiments of the Langley Research Center. Included in this program was a review of projected user requirements for large diameter deployable reflector antennas as well as trade-off studies for the selection of a design concept for 10-meter through 100-meter diameter reflectors. A Hoop/Column concept was selected as the baseline concept. Parametric data are presented in this report for 15-meter, 30-meter, and 100-meter diameters. A 1.82-meter diameter engineering model is described that demonstrated the feasibility of the concept.					
17. Key Words (Suggested by Author(s)) Deployable Reflector Maypole Hoop/Column				18. Distribution Statement Unclassified - Unlimited Subject Category 18	
19. Security Classif. (of this report) Unclassified	20. Security Classif. (of this page) Unclassified		21. No. of Pages 44	22. Price* \$4.00	